Journal of Applied Polymer Science

Linear Segmented Polyurethanes. II. A Mathematical Model for the Prepolymerization Stage

--Manuscript Draft--

Full Title:	Linear Segmented Polyurethanes. II. A Mathematical Model for the Prepolymerization Stage
Manuscript Number:	app.20180495R1
Article Type:	Research Article
Order of Authors:	Mara L. Polo
	Juan I. Pesoa
	Verónica V. Nicolau
	Marisa E. Spontón
	Diana A. Estenoz
	Gregorio R. Meira, Prof.
Manuscript Classifications:	Addition Polymerization; Kinetics; Polyurethane; Theory and Modeling
Additional Information:	
Question	**Response**
Please provide the principal investigator's name and affiliation. (Principal investigator MUST be listed as a co-author on the submission; please DO NOT list all other co-authors in this section.)	Prof. Gregorio R. Meira INTEC (UNL-CONICET)
Please submit a plain text version of your cover letter here. If you also wish to upload a file containing your cover letter, please note it here and upload the file when prompted to upload manuscript files. Please note, if you are submitting a revision of your manuscript, there is an opportunity for you to provide your responses to the reviewers later; please do not add them to the cover letter.	June 21th., 2018 Dr. Brian Knapp Executive Editor Journal of Applied Polymer Science Dear Dr. Knapp: Thank you for your kind reply regarding our manuscript app.20180495: “Linear Segmented Polyurethanes. II. A Mathematical Model for the Prepolymerization Stage”, by M.L. Polo, J.I. Pesoa, V.V. Nicolau, M.E. Spontón, D.A. Estenoz, and G. R. Meira. We agree with all the reviewers’ comments, and we thank them for their help. The new revised version has certainly improved with respect to the original manuscript. In a couple of months, I shall be sending to you the third part of this sequel entitled: “Linear Segmented Polyurethanes. III. A Mathematical Model for the Finishing Stage”, by M.L. Polo, J.I. Pesoa, M.E. Spontón, D.A. Estenoz, and G.R. Meira. Hoping that you may find the corrected manuscript acceptable for publication, please receive my kind regards, Prof. Gregorio R. Meira INTEC (CONICET and Univ. Nac. del Litoral) Güemes 3450 (3000) Santa Fe – Argentina Tel.: 0054-342-451-1370, Ext. 1089 e-mail: gmeira@santafe-conicet.gov.ar

Linear Segmented Polyurethanes. II. A Mathematical Model for the Prepolymerization Stage

Mara L. Polo[1], Juan I. Pesoa[1], Verónica V. Nicolau[2], Marisa E. Spontón[1], Diana A. Estenoz[1], Gregorio R. Meira[1]

[1] INTEC, Universidad Nacional del Litoral and CONICET, (3000) Santa Fe, Argentina.

[2] GPol, Universidad Tecnológica Nacional, Regional San Francisco, (2400) Córdoba, Argentina.

Correspondence to: Gregorio R. Meira (E-mail: *gmeira@santafe-conicet.gov.ar*)

((Additional Supporting Information may be found in the online version of this article.))

ABSTRACT

In the first part of this sequel, an experimental investigation on the synthesis of linear segmented polyurethanes (STPUs) was presented, that included estimation of the kinetic constants at 60 °C for the Prepolymerization and Finishing stages. This work presents two comprehensive mathematical models that simulate the mentioned Prepolymerizations, in reactions between two poly(tetramethylene oxide) PTMO macrodiols and an excess of methylene diphenyl diisocyanate (MDI). The models require to input the molar mass distribution (MMD) of the initial macrodiol. The single-phase (or homogeneous) model calculates a final MMD of approximately 40,000 different molecular species, and somewhat underestimates the observed molar mass dispersities. The double-phases (or heterogeneous) model produces a better fit of the observed MMDs by simulating two independent polymerizations carried out in parallel. The double-phases model contains three adjustable parameters: the reaction imbalances into both phases, and an "effective" rate constant. In Part III of this sequel, the presented models will be extended to simulate the Finishing stages.

INTRODUCTION

Linear Segmented Thermoplastic Polyurethanes (STPUs) are multi-block copolymers typically obtained in two-steps polymerizations.[1,2] In the Prepolymerization, a macrodiol reacts with an excess of diisocyanate to produce a low molar mass prepolymer. In the Finishing stage, a chain extender is added in stoichiometric ratio to produce a high molar mass copolymer. The morphological and thermomechanical characteristics of STPUs are determined by the molecular characteristics acquired during their synthesis, such as the molar mass distribution (MMD), the distribution of hard segments, and the chemical composition distribution.[3–5]

The synthesis of STPUs is still a matter of controversy, due to difficulties introduced by: i) the presence of intramolecular and/or secondary reactions;[6–9] ii) the use of macrodiols;[1] iii) the use of asymmetric diisocyanates;[10–13] iv) the effect of chain length on reaction rate;[14] v) the effect of solvents on reaction rate;[15–17] and vi) the presence of system heterogeneities.[18–22] Consider each of the mentioned difficulties. Intramolecular reactions (yielding molecular cycles), and secondary reactions (yielding allophanates and biuret crosslinking) tend to broaden MMD with respect to the base step reaction mechanism, and their presence depends on the temperature and nature of the reagents.[7,8] The use of polydisperse macrodiols instead of low molar mass diols introduces difficulties for attaining stoichiometric ratios.[1] Asymmetric diisocyanates may exhibit substitution effects and/or differing reactivities in their functional groups. Thus, in reactions between 2,4- and 2,6-tolylene diisocyanate (2,4- and 2,6-TDI) and polypropylene glycol (PPG), Grepinet et al.[13] proposed a kinetic mechanism with six different rate constants; and concluded that 2,4-TDI is 3 times more reactive than 2,6-TDI, while the *para*-isocyanate groups of 2,4-TDI are 6 times more reactive than the *ortho*. In contrast, in reactions between methylene diphenyl diisocyanate (MDI) and 1-butanol (or 1-hexanol) carried out in cyclohexane and in the bulk, Sun and Sung[23], and

Eceiza et al.[24] reported identical reactivities for both isocyanate groups in MDI. On the effects of chain length, Król[14] assumed a variation of the reaction rate with the molar mass, on the basis of a collision theory and model reactions between aromatic/aliphatic isocyanates and alcohols or hydroxyethers. On the effects of solvents, Chang and Chen[15] proposed an ion-pair mechanism, where first the alcohol group forms a hydrogen bonding complex with the isocyanate, and then an aprotic solvent solvates the active hydrogen in the complex and generates an ion pair that facilitates urethane formation. Moreover, the electron donation capability of the solvent may either enhance or diminish reaction rate.[15] Regarding reaction heterogeneities, several articles have reported premature phase separations in the synthesis of polyurethanes.[18–22] For bulk and one-step reactions between MDI, a poly(propylene oxide) capped with poly(ethylene oxide) diol (PPO-PEO), and 1,4-butanediol (BD), and on the basis of viscosity and turbidity measurements, Castro et al.[18] concluded that phase separations occurred when the hard-segment sequences generated from MDI and BD reach an average chain length of 1.3 or higher. Subsequent measurements by Hager et al.[19] (employing differential scanning calorimetry), and by Camargo et al.[20] (employing Fourier transform infrared spectroscopy), confirmed premature phase separations in the same reaction systems, possibly again due to segregation of the longer hard segments. Segregation occurs either because the hard segments become increasingly incompatible with the soft segments, or because of the propensity of hard segments to crystallize.[18–20] Similarly, MacKnight and coworkers[21,22] provided strong evidence of macroscopic phase separations in bulk two-steps reactions between 2,4- or 2,6-TDI, a hydroxyl-terminated polybutadiene (HTPB), and BD. When BD was added in the Finishing stage, it was seen to immediately form a separate phase. And since this behavior was observed with both crystallizable and non-crystallizable hard segments, it was concluded that phase separation was caused by reactants incompatibility rather than by crystallization.[21,22]

Moreover, the final polymers exhibited bimodal distributions of hard segment sequences and broad MMDs. This suggests a blend of hard- and soft-segment-rich materials; with the hard-segment-rich materials produced by diffusion of the diisocyanate into the BD droplets.[21,22] For the bulk one-step reaction between MDI, PEO-PEG, and BD (and in accordance with Refs[18–20]) MacKnight and coworkers[21,22] also noted that the macroscopic phase separation did not occur immediately after addition of BD, but rather at a later point.

The mathematical modeling of step-growth polymerizations has been an active field of research along many decades.[25–38] The developed models may be classified as stochastic[25–38] or deterministic[30,32,33,35–38]. Stochastic models are typically represented by algebraic equations, and predict the evolution of the MMD along the extent of reaction. Deterministic models require to input reaction rate, are typically represented by sets of differential equations, and the independent variable is time. Due to lack of computational facilities, the first models have been all stochastic,[25] and adopted the following "classical" (equal reactivity) assumptions:[25,30–33,36–38] i) intramolecular or secondary reactions are negligible; ii) the reaction rate is independent of chain length; and iii) the polymerization is homogeneous. When applying such assumptions onto standard AA + BB polymerizations carried out to high conversion, the following is observed: a) under stoichiometric conditions, the MMD tends to a "most probable" (or Schulz-Flory) distribution of molar mass dispersity $\bar{M}_{\mathrm{w}}/\bar{M}_{\mathrm{n}} \to 2$;[25] and b) under non-stoichiometric conditions, lower average molar masses and dispersities are obtained. Later publications have relaxed the mentioned assumptions. For example, Nanda and Jain[26] adopted a linear dependence between the rate constant and the chain length, and showed that the molar mass dispersity results in a value that is lower than 2 when the reactivity decreases with chain length, or higher than 2 when it increases.

Table 1 compare many of the articles that contain mathematical models for the synthesis of STPU's, with the aim of predicting MMDs and averages. The models are grossly classified into 2 main groups, according to whether they simulate the synthesis of oligomers[1,13,39–44] or high polymers.[1,45–54] The reason for such classification is the greatly increased number of different molecular types in high polymers. In Table 1, the typical two-steps processes (*i.e.*: a non-stoichiometric Prepolymerization followed by a stoichiometric Finishing stage) are represented by recipes ii) and iii), respectively.

TABLE 1

Several of the articles in Table 1 have relaxed the "classical" assumptions as follows: i) by imposing different reactivities onto both –NCO groups of diisocyanates;[13,39,40,43,44,46,47,49,50] ii) by imposing different reactivities for the –OH groups of the macrodiol with respect to –OH groups in the chain extender;[48,49,52,53] iii) by simulating a system heterogeneity;[51–53] and iv) by imposing a chain-length-dependent rate of reaction.[42] Except for the last item, all the other extensions from classical assumptions tend to broaden MMD; and several solutions have been proposed for simulating such broadenings.[39,40,48,51–53] For example, Gandhi and Babu[39] modelled the reaction of a symmetric diisocyanate assuming different reactivities for the –NCO groups in the monomer with respect to the –NCO groups in the growing oligomers. Similarly, for polymerizations between an asymmetric monomer and its induced products, Gandhi and Babu[40] adopted a reaction mechanism with four different rate constants. Later, Lopez-Serrano et al.[48] assumed different rate constants for the –OH groups in the macrodiol with respect to the –OH groups in the chain extender. Finally, for the one-step synthesis of high polymers, Miller et al.[51,52] and Speckhard et al.[53] simulated a reaction heterogeneity through an equivalent two-phases polymerization where both phases are assumed homogeneous but with different initial concentrations, and the total

mixture is obtained by addition of the mixtures in both phases. More specifically, the macrodiol and the diisocyanate were partitioned into a macrodiol-rich phase and a diisocyanate-rich phase, and the chain extender was distributed between the phases to ensure stoichiometry.[51–53]

The deterministic models developed in the present work simulate the MMDs of the relatively low molar mass polymers obtained in non-stoichiometric Prepolymerizations, and are comparable to the models in Refs[13,39–44] (Table 1). Gandhi and Babu[39] investigated the kinetics of a step polymerization of a comonomer with unequal reactivities, and calculated the molar mass dispersity along conversion and as a function of the initial stoichiometry. Later, Gandhi and Babu[40] investigated the kinetics of a step polymerization between a symmetric comonomer and a difunctional comonomer with non-equivalent reactivities. Employing the models of Refs,[39,40] Grepinet et al.[13] simulated a non-stoichiometric bulk polymerization between PPG and a mixture of asymmetric 2,4- and 2,6-TDI, and estimated the mass concentration of the oligomers containing 1 and 2 sequences of PPG in each chain, but without estimating the MMD. Finally, the models by Król and coworkers[41–44] estimate the MMDs of the oligomers obtained at low conversions in stoichiometric reactions between 2,4-TDI and BD, but without including macrodiols.

In the first part of this sequel,[1] five polymerizations were carried out at 60 °C between MDI, two different PTMO macrodiols, and BD. The Prepolymerizations were in bulk, and the Finishing stages were in THF solution. At the Prepolymerization ends, the reaction mixtures only contained unreacted MDI and a distribution of isocyanate-capped oligomers. The Finishing stages were started after addition of the chain extender in global stoichiometric ratios. For Exp. 1, ^{1}H-NMR was used to estimate the number of moles of unreacted isocyanate groups and generated urethane groups along the Prepolymerization and Finishing stages; and those measurements were employed

to adjust the rate constant of each reaction stage. However, such adjustments did not include the MMD measurements by size exclusion chromatography (SEC).[1]

In this work, two comprehensive mathematical models are presented for simulating the Prepolymerizations of Exps 1-5 described in Polo et al.[1] The new models readopt the classical assumptions by Flory[25] of irreversible and intermolecular reactions, equal reactivity, and system homogeneity. Employing the Prepolymerization rate constant reported in Polo et al.[1], the homogeneous (or single-phase) model adequately predicts the evolution of the $\bar{M}_n$ measurements of the global reaction mixture, but underestimates the $\bar{M}_w$ measurements of the total polymer. The double-phases model aims at better simulating the observed MMDs; and to this effect it emulates a reaction heterogeneity by assuming two independent homogeneous polymerizations carried out in parallel.

GENERAL CONSIDERATIONS

Reaction Scheme, Nomenclature, and Global Variables

Table 2 presents the Prepolymerization scheme, and the employed nomenclature. The following symbols describe any polymer species type contained in the reaction mixture:

$$P_{x,R}^{AA} \quad , \quad P_{x,R}^{BA} \quad , \text{ and } \quad P_{x,R}^{BB}, \text{ with } \quad (x, R = 1, 2, ...)$$

where the superscripts A (≡ –NCO) and B (≡ –OH) represent the chemical natures of the end groups; subscript *x* represents the number of soft MDI-macrodiol sequences; and subscript *R* represents the total number of macrodiol repeating units. Note the following: i) $P_{1,R}^{BB}$ with (R = 1, 2, …) represents the unreacted (PTMO) macrodiol; and ii) the unreacted MDI is not considered a polymer species, and is represented by MDI^{AA}, to highlight the chemical nature of its end groups.

TABLE 2

While the polymer species are specified by four parameters (A, B, x, R), the polymer topologies are specified by only three parameters (A, B, x), as follows:

$$\mathrm{P}_x^{\mathrm{AA}} \quad , \quad \mathrm{P}_x^{\mathrm{BA}} \quad , \text{ and } \quad \mathrm{P}_x^{\mathrm{BB}}, \text{ with } \quad (x = 1, 2, \ldots)$$

Thus, while any molecular species exhibits a single molar mass, a polymer topology exhibits a whole distribution of molar masses at intervals of the PTMO repeating unit.

Call P^{AA}, P^{BA}, and P^{BB} the subsets of polymer species containing AA, BA, and BB end groups, respectively, for all the possible combinations of (x, R). Also, call P the complete set of polymer species. Finally, [z] (in mol L^{-1}) and c_z (in g L^{-1}) respectively represent the molar and mass concentrations of any generic species or set of species z. Thus, one can write:

$$\left[\mathrm{P}_x^{\mathrm{BA}}\right] = \sum_{\forall R} \left[\mathrm{P}_{x,R}^{\mathrm{BA}}\right] \qquad (x, R = 1, 2, \ldots) \quad (1)$$

$$\left[\mathrm{P}^{\mathrm{BA}}\right] = \sum_{\forall x} \sum_{\forall R} \left[\mathrm{P}_{x,R}^{\mathrm{BA}}\right] \qquad (x, R = 1, 2, \ldots) \quad (2)$$

$$\left[\mathrm{P}\right] = \sum_{\forall x} \sum_{\forall R} \left[\mathrm{P}_{x,R}^{\mathrm{AA}}\right] + \sum_{\forall x} \sum_{\forall R} \left[\mathrm{P}_{x,R}^{\mathrm{BA}}\right] + \sum_{\forall x} \sum_{\forall R} \left[\mathrm{P}_{x,R}^{\mathrm{BB}}\right] \qquad (x, R = 1, 2, \ldots) \quad (3)$$

$$c_{\mathrm{P}_x^{\mathrm{BA}}} = \sum_{\forall R} c_{\mathrm{P}_{x,R}^{\mathrm{BA}}} \qquad (x, R = 1, 2, \ldots) \quad (4)$$

$$c_{\mathrm{P}^{\mathrm{BA}}} = \sum_{\forall x} \sum_{\forall R} c_{\mathrm{P}_{x,R}^{\mathrm{BA}}} \qquad (x, R = 1, 2, \ldots) \quad (5)$$

$$c_{\mathrm{P}} = \sum_{\forall x} \sum_{\forall R} c_{\mathrm{P}_{x,R}^{\mathrm{AA}}} + \sum_{\forall x} \sum_{\forall R} c_{\mathrm{P}_{x,R}^{\mathrm{BA}}} + \sum_{\forall x} \sum_{\forall R} c_{\mathrm{P}_{x,R}^{\mathrm{BB}}} \qquad (x, R = 1, 2, \ldots) \quad (6)$$

The molar masses of $\mathrm{P}_{x,R}^{\mathrm{AA}}$, $\mathrm{P}_{x,R}^{\mathrm{BA}}$, and $\mathrm{P}_{x,R}^{\mathrm{BB}}$ are represented by $M_{\mathrm{P}_{x,R}^{\mathrm{AA}}}$, $M_{\mathrm{P}_{x,R}^{\mathrm{BA}}}$, and $M_{\mathrm{P}_{x,R}^{\mathrm{BB}}}$, respectively; and their expressions are given by Eqs (A.1)-(A.3) in Appendix A. The mass concentration of any generic $\mathrm{P}_{x,R}^{\mathrm{BA}}$ species is obtained from its molar concentration through:

$$c_{\mathrm{P}_{x,R}^{\mathrm{BA}}} = \left[\mathrm{P}_{x,R}^{\mathrm{BA}}\right] \times M_{\mathrm{P}_{x,R}^{\mathrm{BA}}} \qquad (x, R = 1, 2, \ldots) \quad (7)$$

The number and weight MMDs are represented by the discrete functions $\left[\mathrm{P}_i\right](M_i)$ and $c_{\mathrm{P}_i}(M_i)$, respectively; where P_i with (i = 1, 2, …) are hypothetical polymer species of molar masses M_i at multiples of the PTMO repeating unit (ΔM = 72 g mol^{-1}). The number and weight MMDs were calculated as follows, by adding the concentrations of all the polymer species contained in the ranges [($M_i - \Delta M/2$), ($M_i + \Delta M/2$)]:

$$\left[\mathrm{P}_i\right](M_i) = \sum_{M_i-\Delta M/2}^{M_i+\Delta M/2}\left[\mathrm{P}_{x,R}^{\mathrm{AA}}\right](M_{\mathrm{P}_{x,R}^{\mathrm{AA}}}) + \sum_{M_i-\Delta M/2}^{M_i+\Delta M/2}\left[\mathrm{P}_{x,R}^{\mathrm{BA}}\right](M_{\mathrm{P}_{x,R}^{\mathrm{BA}}}) + \sum_{M_i-\Delta M/2}^{M_i+\Delta M/2}\left[\mathrm{P}_{x,R}^{\mathrm{BB}}\right](M_{\mathrm{P}_{x,R}^{\mathrm{BB}}}) \qquad (x, R, i = 1, 2, ...) \quad (8)$$

$$c_{\mathrm{P}_i}(M_i) = \sum_{M_i-\Delta M/2}^{M_i+\Delta M/2} c_{\mathrm{P}_{x,R}^{\mathrm{AA}}}(M_{\mathrm{P}_{x,R}^{\mathrm{AA}}}) + \sum_{M_i-\Delta M/2}^{M_i+\Delta M/2} c_{\mathrm{P}_{x,R}^{\mathrm{BA}}}(M_{\mathrm{P}_{x,R}^{\mathrm{BA}}}) + \sum_{M_i-\Delta M/2}^{M_i+\Delta M/2} c_{\mathrm{P}_{x,R}^{\mathrm{BB}}}(M_{\mathrm{P}_{x,R}^{\mathrm{BB}}}) \qquad (x, R, i = 1, 2, ...) \quad (9)$$

The average molar masses for the polymer alone ($\bar{M}_{\mathrm{n,P}}$, $\bar{M}_{\mathrm{w,P}}$) and for the global reaction mixture that includes the unreacted MDI ($\bar{M}_{\mathrm{n,G}}$, $\bar{M}_{\mathrm{w,G}}$) were directly calculated through Eqs (A.4)-(A.7) in Appendix A. Finally, Equations (A.8)-(A.13) in Appendix A calculate the number of moles and molar concentrations of unreacted end groups and generated urethane groups, represented by ($n_{\mathrm{-NCO}}$, $n_{\mathrm{-OH}}$, $n_{\mathrm{-NHCOO-}}$) and ([–NCO], [–OH], [–NHCOO–]), respectively.

Measurements by Polo et al.[1] and the Basic Global Model

Consider the Prepolymerizations of Exps 1-5 in Polo et al.[1] The upper sections of Table 3 reproduce the recipes and the following measurements at the final reaction times (t_{end}): average molar masses of the polymer alone ($\bar{M}_{\mathrm{n,P}}$, $\bar{M}_{\mathrm{w,P}}$), weight fraction of unreacted MDI (ω_{MDI}), and average molar masses of the global reaction mixture ($\bar{M}_{\mathrm{n,G}}$, $\bar{M}_{\mathrm{w,G}}$). The final reaction times (t_{end}) were adopted at extents of reaction close to unity, when the measured variables reach steady-state values.

TABLE 3

The new mathematical models require to input the discrete number MMD of the initial macrodiol; and Figure 1 presents the SEC estimates of the employed prepolymers: $PTMO_1$ and $PTMO_2$.[1] The MMDs of $PTMO_1$ and $PTMO_2$ contain 221 and 604 points, respectively; with points at multiples of 72 g mol^{-1}.

From the measurements at $t = t_{end}$, note the following (Table 3): a) the molar mass dispersities of the polymers alone ($\bar{M}_{w,P}/\bar{M}_{n,P}$) are all higher than 2; and b) the molar mass dispersities of the global mixtures ($\bar{M}_{w,G}/\bar{M}_{n,G}$) are all higher than 3.

FIGURE 1

For Exp. 1, the points in Figure 2 represent the measurements at several reaction times.[1] Figure 2a presents the measured number of moles of isocyanate and urethane groups, and two estimates for the moles of –OH groups obtained from the former measurements. Figures 2b and 2c present the measured average molar masses of the polymer alone and of the global reaction mixture. The last averages of the total reaction mixture ($\bar{M}_{n,G}$, $\bar{M}_{w,G}$) were calculated from ($\bar{M}_{n,P}$, $\bar{M}_{w,P}$) and the weight fractions of unreacted MDI (ω_{MDI}), through:[1]

$$\frac{1}{\bar{M}_{n,G}(t)} = \frac{\omega_{MDI}(t)}{M_{MDI}} + \frac{\left[1-\omega_{MDI}(t)\right]}{\bar{M}_{n,P}(t)} \tag{10a}$$

$$\bar{M}_{w,G}(t) = \omega_{MDI}(t) \times M_{MDI} + \left[1-\omega_{MDI}(t)\right] \times \bar{M}_{w,P}(t) \tag{10b}$$

with M_{MDI} = 250.25 g mol^{-1}.

Figure 2d presents the experimental values of the extent of reaction (p) at several reaction times, calculated through:

$$p(t) = \frac{n^0_{-OH} - n_{-OH}(t)}{n^0_{-OH}} \tag{11}$$

where n^0_{-OH} are the initial moles of –OH groups (= 0.00365 in Exp. 1); and n_{-OH} are the measured moles of –OH groups (Figure 2a).

FIGURE 2

In Polo et al.[1], a Prepolymerization rate constant based on the number of moles was adjusted to fit the measurements of Figure 2a, yielding ($k'_{1,I} = 0.307$ mol^{-1} s^{-1}). To that effect, the following global model was employed:

$$\frac{dn_{-OH}(t)}{dt} = -k'_{1,I}[n_{-NCO}(t) \times n_{-OH}(t)] \quad (12a)$$

$$\frac{dn_{-NCO}(t)}{dt} = -k'_{1,I}[n_{-NCO}(t) \times n_{-OH}(t)] \quad (12b)$$

$$\frac{dn_{-NHCOO-}(t)}{dt} = k'_{1,I}[n_{-NCO}(t) \times n_{-OH}(t)] \quad (12c)$$

where n^0_{-OH} (= 0.00365), n^0_{-NCO} (= 0.0121), and $n^0_{-NHCOO-}$ (= 0) are the initial moles of –OH, –NCO, and –NHCOO– groups. When based on molar concentrations (instead of on the number of moles), the rate constant resulted in: $k_{1,I} = 0.00107$ L mol^{-1} s^{-1}.[1] The solutions of Eqs (12) with $k'_{1,I}$ are represented in continuous trace in Figure 2a. In Figure 2d, a theoretical time function for the extent of reaction was obtained by replacing the solution for $n_{-OH}(t)$ of Eq. (12a) into Eq. (11). As we shall see later, the solutions of Eqs (11)-(12) in Figures 2a,d coincide with the results by the single-phase model employing the same rate constant. Figures 2e-g reproduce the measurements and model predictions of Figures 2a-c, but *vs* the extent of reaction, as transformed through the continuous $p(t)$ function of Figure 2d. As expected from the definition of Eq. (11), the theoretical predictions of Figures 2e show linear relationships between the number of moles and the extents of reaction.

Finally, the following classical expression[25] was employed to calculate the continuous $\bar{M}_{n,G}(p)$ function of Figure 2g:

$$\bar{M}_{n,G}(p) = \bar{M}^{0}_{n,G} \times \frac{1+r'}{1+r'-2\,r'\,p} \tag{13a}$$

with

$$r' = \frac{n^{0}_{-OH}}{n^{0}_{-NCO}} \leq 1 \tag{13b}$$

$$\bar{M}^{0}_{n,G} = \frac{n^{0}_{-NCO} \times M_{MDI} + n^{0}_{-OH} \times \bar{M}_{n,PTMO}}{n^{0}_{-NCO} + n^{0}_{-OH}} \tag{13c}$$

where r' (= 0.3) is the recipe imbalance, or ratio between the initial number of end groups in defect and the initial number of end groups in excess; p is an independent variable that was varied between 0 and 1; $\bar{M}^{0}_{n,G}$ (= 395 g mol^{-1}) is the number-average molar mass of the initial reaction mixture; $\bar{M}_{n,PTMO}$ (= 876 g mol^{-1}) is the number-average molar mass of the initial PTMO; and M_{MDI} = 250.25 g mol^{-1}. The $\bar{M}_{n,G}(p)$ function calculated through Eqs (13) also coincides with the single-phase model prediction.

SINGLE-PHASE (OR HOMOGENEOUS) MODEL

Consider the reaction mechanism of Table 4. It considers (at molecular species level) all the possible reactions between A and B groups contained in different molecules. The corresponding mass balance is given by Eqs (B.1)-(B.4) in Appendix B. The single-phase (or homogeneous) model readopts the Prepolymerization rate constant of Polo et al.,[1] and consists of Eqs (1)-(11), (A.1)-(A.13), and (B.1)-(B.4). Its numerical solution provides the time evolution of the generated polymer species and unreacted reagents. The computational flow-sheet is presented in the Supplementary Information (Table S1). The computer program was written in MatLab®, and the

differential equations (B.1)-(B.4) were solved through a Forward-Euler discretization procedure, and employing a constant time step of 1 s. The simulation of a typical Prepolymerization experiment required about 2 hrs of computation time. At the Prepolymerization end, around 40,000 different molecular types were calculated, with 11% of them representing over 99% of the total reaction mass.

TABLE 4

For Exp. 1, the simulation results are presented in Figures 2 and 3. In Figures 2,a,d,e, the results by the single-phase model coincide with the results of Eqs (11)-(13), since both models are based on the same "classical" assumptions. Note the following: a) the (time and extent of reaction) functions for $\bar{M}_{n,P}$, $\bar{M}_{w,P}$, and $\bar{M}_{w,G}$ in Figures 2b,c,f,g cannot be estimated *via* simple global models; b) the simulation results of Figures 2e-g are independent of the kinetic constant value; and c) in Figures 2c,d, the single-phase model predictions for $\bar{M}_{n,G}(t)$ and $p(t)$ properly fit the measurements, since both functions are indirectly based on the well-adjusted $n_{-OH}(t)$ function of Figure 2a.

FIGURE 3

For Exp. 1, Figures 3a-f present the single-phase model predictions for the weight MMDs of the total polymers at reaction times 2, 7, and 30 min. In such figures, the individual polymer species are classified together into their corresponding topologies. In Figures 3a-c, the weight MMDs are represented with linear horizontal axes; and with points at constant molar mass intervals ΔM = 72 g mol^{-1}. In Figures 3d-f, the same distributions are represented with logarithmic horizontal axes, and with points at variable $\Delta \log M$ intervals. Finally, Figures 3g-i compare the measurements an model predictions for the weight MMDs and weight fractions of unreacted MDI.

For the complete set of Exps 1-5, Table 3, section a) presents the single-phase model predictions for the average molar masses and extents of reaction at their t_{end} values. Note that while the final values of $\bar{M}_n$ for the global mixtures ($\bar{M}_{n,G}$) are all reasonably well predicted, the final polymer dispersities ($\bar{M}_{w,P}/\bar{M}_{n,P}$) are all underestimated, and so are the corresponding $\bar{M}_w$ values ($\bar{M}_{w,P}$).

DOUBLE-PHASES (OR HETEROGENOUS) MODEL

Proposed Method

In order to better predict the observed MMDs and averages, a crude double-phases model was developed that assumes two independent homogeneous polymerizations carried out in parallel, with different initial imbalances, and with the total mixture obtained by addition of the mixtures in both phases. The double-phases model applies the single-phase model onto each phase, and for this reason the total number of evolving molecular species approximately doubles that of the single-phase model. However, most of the generated polymer species are common to both phases, and therefore the final number of species is only a little higher than in the single-phase model.

The aim of the double-phases model is to predict the final measurements of $\bar{M}_{w,P}$ at t_{end}, while not affecting the (already correct) single-phase model predictions of $\bar{M}_{n,G}$ at t_{end} (see Table 3). Let us identify the reaction phases 1 and 2 with the subindexes 1 and 2, respectively. The initial moles of reactive end groups (n^0_{-OH}, n^0_{-NCO}) are split into phases 1 and 2, as follows:

$$n^0_{-OH} = n^0_{-OH,1} + n^0_{-OH,2} \tag{14a}$$

$$n^0_{-NCO} = n^0_{-NCO,1} + n^0_{-NCO,2} \tag{14b}$$

The following requirements are imposed onto the split of reagents: a) the imbalance of phase 1 is lower than the global imbalance, and the imbalance of phase 2 is higher than the global imbalance; and b) like in the global recipe, both phases contain an excess of MDI. Thus, one can write:

$$r'_1 \le r' \le r'_2 \tag{15a}$$

with

$$r'_1 = \frac{n^0_{-\mathrm{OH},1}}{n^0_{-\mathrm{NCO},1}} = \frac{n^0_{\mathrm{PTMO},1}}{n^0_{\mathrm{MDI},1}} \le 1 \quad ; \quad r'_2 = \frac{n^0_{-\mathrm{OH},2}}{n^0_{-\mathrm{NCO},2}} = \frac{n^0_{\mathrm{PTMO},2}}{n^0_{\mathrm{MDI},2}} \le 1 \tag{15b}$$

Along the reaction, it is:

$$n_{-\mathrm{OH}}(t) = n_{-\mathrm{OH},1}(t) + n_{-\mathrm{OH},2}(t) \tag{16a}$$

$$n_{-\mathrm{NCO}}(t) = n_{-\mathrm{NCO},1}(t) + n_{-\mathrm{NCO},2}(t) \tag{16b}$$

The individual and global extents of reaction are defined by:

$$p_1(t) = \frac{n^0_{-\mathrm{OH},1} - n_{-\mathrm{OH},1}(t)}{n^0_{-\mathrm{OH},1}} \quad ; \quad p_2(t) = \frac{n^0_{-\mathrm{OH},2} - n_{-\mathrm{OH},2}(t)}{n^0_{-\mathrm{OH},2}} \tag{17a}$$

$$p(t) = \frac{n^0_{-\mathrm{OH}} - n_{-\mathrm{OH}}(t)}{n^0_{-\mathrm{OH}}} = 1 - X^0_{-\mathrm{OH},1}\left[1 - p_1(t)\right] - X^0_{-\mathrm{OH},2}\left[1 - p_2(t)\right] \tag{17b}$$

where $X^0_{-\mathrm{OH},1}$ and $X^0_{-\mathrm{OH},2}$ are the initial molar fractions of –OH end groups in phases 1 and 2, respectively. Note that while phase 1 contains a larger excess of MDI than the global recipe, phase 2 is closer to stoichiometric equilibrium. Thus, at a common final time and compared to phase 2, phase 1 reaches a higher extent of reaction and produces a lower molar mass polymer. This is because: a) the upper limit of the average molar mass is reduced when lowering the imbalance; and b) the rate of consumption of –OH groups increases when increasing the excess of MDI. Note the following: a) the single-phase model solution is recuperated with $r'_1 = r'_2 = r'$; and b) by increasing the difference between r'_1 and r'_2, one also increases the differences in the average molar

masses and extents of reaction in the corresponding phases. In order to make the split of reagents independent of the global imbalance r', it is convenient to adjust the following fractional variations of the global imbalance:

$$\frac{\Delta r'_1}{r'} = \frac{r' - r'_1}{r'} \geq 0 \tag{18a}$$

$$\frac{\Delta r'_2}{r'} = \frac{r' - r'_2}{r'} \leq 0 \tag{18b}$$

After adjustment of $(\Delta r'_1/r',\ \Delta r'_2/r')$, Eqs (18) calculate the phase imbalances $(r'_1,\ r'_2)$ for any given total imbalance r'.

By increasing the difference between r'_1 and r'_2 at high extents of reaction, one increases the value of $\bar{M}_w$ produced in phase 2 ($\bar{M}_{w,P,2}$), and consequently one also increases the value of the total $\bar{M}_{w,P}$. However, the split of reagents does not affect the already well fit functions: $n_{-NCO}(p)$, $n_{-OH}(p)$, $n_{-NHCOO-}(p)$, and $\bar{M}_{n,G}(p)$. To prove that $\bar{M}_{n,G}(p)$ remains unaffected by the split of reagents, see Appendix C.

The $p(t)$ function predicted by the double-phases model through Eq. (17b) is clearly affected by the rate constant value; and in general will not coincide with the $p(t)$ function predicted by the single-phase model. For this reason, the double-phases model will not generally predict the required value of $\bar{M}_{w,P}$ at t_{end}. Thus, the following 2-steps adjustment procedure is proposed: 1) select the split of reagents with $k_{1,I}$, in order to predict the desired value of $\bar{M}_{w,P}$ at a high extent of reaction; and 2) contract or expand all time functions by modifying the rate constant value into $k_{1,II}$, in order to predict the required value of $\bar{M}_{w,P}$ at t_{end}.

Model Adjustment and Simulation Results for Exp. 1

The described procedure was applied onto the measurements of Exp. 1, with the aim of predicting the measurement $\bar{M}_{w,P,Exp.}$ = 3540 g mol^{-1} at t_{end} = 30 min. (see Table 3); while not affecting the well adjusted functions $n_{-NCO}(p)$, $n_{-OH}(p)$, $n_{-NHCOO-}(p)$, and $\bar{M}_{n,G}(p)$. The final results are in dot-dashed trace in Figure 4. Figure 4 maintains the general structure of Figure 2, and also includes the simulation results by the single-phase model (in continuous trace), and the result of step 1 of the double-phases model (in dashed trace).

FIGURE 4

In step 1 with $k_{1,I}$, the fractional variations of the imbalances ($\Delta r'_1/r'$, $\Delta r'_2/r'$) were adjusted to predict the experimental value of $\bar{M}_{w,P}$ (= 3540 g mol^{-1}) at a high extent of reaction (but not necessarily at t_{end} = 30 min.). With the restrictions of Eqs (18), Figure 5 illustrates the global search that was implemented to find the values of $\Delta r'_1/r'$ and $\Delta r'_2/r'$, that predict the sought value of $\bar{M}_{w,P,Exp.}$ at a high extent of reaction. In Figure 5, E% represents the fractional error:

$$E\% = \frac{\bar{M}_{w,P,Exp} - \bar{M}_{w,P,Theor.}}{\bar{M}_{w,P,Exp}} \times 100 \qquad (19)$$

where $\bar{M}_{w,P,Theor.}$ is the model prediction. The set of solutions with E% = 0 % is shown in continuous trace in Figure 5. From all the possible solutions, point C was arbitrarily chosen at ($\Delta r'_1/r'$ = 0.567, $\Delta r'_2/r'$ = -0.643), or equivalently with (r'_1 = 0.130, r'_2 = 0.494). The solutions for step 1 with $k_{1,I}$ = 0.00107 g mol^{-1} and the mentioned values of r'_1 and r'_2, are represented in dashed trace in Figure 4. Note that as expected, $\bar{M}_{w,P}$ reaches 3540 g mol^{-1} at a high extent of reaction (Figure 4f), but at t = 80 min. instead of at t_{end} = 30 min. (Figure 4b). Moreover, the split

of reagents slows down all the time functions with respect to the single phase case [compare in Figure 4d, the continuous and dashed curves of $p(t)$].

FIGURE 5

In Step 2, the kinetic constant was readjusted to produce the correct value of $\bar{M}_{w,P}$ at t_{end} = 30 min., yielding $k_{1,II}$ = 0.00265 L mol^{-1} s^{-1}; and the corresponding solutions are shown in dot-dashed trace in Figure 4. As expected, the functions $n_{-NCO}(p)$, $n_{-OH}(p)$, $n_{-NHCOO-}(p)$, and $\bar{M}_{n,G}(p)$ of Figures 4e,g remain unaffected by the adjustment procedure; while the following functions were modified with respect to the single-phase model solutions: $\bar{M}_{w,P}(t)$, $\bar{M}_{n,P}(t)$, and $\bar{M}_{w,G}(t)$ (Figures 4b and 4c). Figure 4b shows that while the double-phases model adequately predicts $\bar{M}_{w,P}(t_{end})$, the prediction for $\bar{M}_{n,P}(t_{end})$ shows a greater deviation from the measurement than the single-phase model prediction. Also, compared to the single-phase model, the double-phases model produces better predictions for $\bar{M}_{w,G}(t_{end})$ (Figure 4c). Figure S1 in the Supplementary Information reproduces the solutions of the single-phase model and of step 2, but including the evolutions of the different variables in phases 1 and 2.

Figures 6 and 7 present further simulation results for Exp. 1. Figure 6 presents the time evolution of the total masses of reagents and main polymer topologies, obtained by addition of the products of phases 1 and 2. Figure 6a presents the evolutions of the unreacted MDI, total polymer, and subsets P of polymer species with end groups BA, AA, and BB. The following is observed: i) the mass of P^{BB} molecules with –OH groups falls monotonically to zero; ii) the mass of P^{BA} molecules first reaches a maximum and then tends to zero; and iii) the mass of P^{AA} monotonically increases to a final plateau that represents the total polymer mass, and the mass of unreacted MDI (MDI^{AA}) monotonically falls to a final constant value. In Figures 6b-d, $P^{BA}(t)$, $P^{AA}(t)$, and $P^{BB}(t)$ are shown

decomposed into their main contributing topologies, noting that $P^{BB}(t)$ mainly consists of unreacted PTMO.

Finally, Figure 7 presents the measured and predicted final MMDs of the total polymer and main topologies at t_{end} = 30 min. Note the following: a) each polymer topology exhibits a fixed normalized MMD, with fixed average values; b) the most abundant polymer topology ($P_{1,R}^{AA}$) contains a single PTMO sequence and two isocyanate end groups; and c) the higher topologies with $x \geq 5$ are responsible for the increase in the global value of $\bar{M}_{w,P}$.

FIGURES 6 and 7

Application of the Adjusted Model onto Exps 2 to 5

Without any other further adjustment, the adjusted model for Exp. 1 (i.e., with $\Delta r'_1/r'$ = 0.567, $\Delta r'_2/r'$ = -0.643, and $k_{1,II}$ = 0.00265 L mol^{-1} s^{-1}) was directly applied to simulate the other 4 experiments, and the final results are presented in Figure 8 and Table 3, section b). The first rows of Table 3, section b) show the resulting splits into phases 1 and 2 (r'_1, r'_2), the initial molar fractions of –OH end groups in phases 1 and 2 ($X^0_{-OH,1}$, $X^0_{-OH,2}$), and the weight fractions in phases 1 and 2 (ω_1, ω_2). Figure 8 presents the measurements and model predictions for the weight MMDs at t_{end}; and Table 3, section b) shows the final values of the extents of reaction and average molar masses for phases 1 and 2 and for the total mixture. In Figure 8, the predicted MMDs are composed by 2 distributions: a lower MMD produced in phase 1, and a higher MMD produced in phase 2. Note the following: a) the total predicted distributions simulate reasonably well the shapes of the measured distributions, showing coincidence with the elbows observed at low molar masses; b) as expected, the global extents of reaction and average molar masses are intermediate between the corresponding values in phases 1 and 2; and c) for the final polymers, the predicted molar mass

dispersities ($\bar{M}_{w,P}/\bar{M}_{n,P}$) are in general lower than the measurements, but higher than the single-phase model predictions.

FIGURE 8

CONCLUSIONS

This article presents three mathematical models for simulating the Prepolymerization stage in the synthesis of STPUs: a simple global model partially presented in Polo et al.[1], and two novel comprehensive models: the single-phase and double-phases models. All of these models readopt the classical equal reactivity assumptions. The global and single-phase models contain a single adjustable parameter: the kinetic constant $k_{1,I}$. The double-phases model includes two additional parameters for the split of reagents into both reaction phases. The double-phases model aims at simulating the effects that tend to broaden the MMD with respect to the classical solution, such as the presence of intramolecular or secondary reactions, segregation by imperfect mixing, and/or the presence of phase separations. The real causes of the MMD broadening remain unknown.

As far as the authors are aware, the presented (single- and double-phases) models are the first in the literature that calculate the evolution of all the molecular species generated along non-stoichiometric Prepolymerizations that include macrodiols. In both models, each molecular species is characterized by its accurately-calculated molar mass.

The double-phases model was adjusted to the measurements of Exp. 1, and the resulting adjustment was then applied onto Exps. 2-5, with reasonably good results. Clearly, a better overall adjustment would involve the measurements of all 5 experiments. Furthermore, in step 1, many combinations of the fractional imbalances ($\Delta r'_1/r'$, $\Delta r'_2/r'$) predict the sought value of $\bar{M}_{w,P}$ at a high extent of reaction, but point C in Figure 5 was arbitrarily selected. Thus, this adjustment step could be improved by simultaneously requiring better estimates for some other variable such

as the corresponding number-average molar mass $\bar{M}_{n,P}$. Similarly, in step 2, a better overall rate constant could be adjusted by considering the complete time evolution of $\bar{M}_{w,P}$, rather than only its value at t_{end}.

With relatively little extra effort, the reaction scheme could be extended to include other non-classical effects such as different reactivities in asymmetric diisocyanates and the generation of cyclic species. In the third part of this sequel, the presented models are extended to simulate the Finishing stage, that starts after addition of the chain extender

ACKNOWLEDGMENTS

The authors wish to thank CONICET (Grant N° PIP2011 848 and Grant N° PUE2016 007), and Universidad Nacional del Litoral (Grant N° CAI+D2011 454) for the project funding.

APPENDIX A: MOLAR MASSES AND GLOBAL MOLAR CONCENTRATIONS

The following expressions calculate the molar masses ($M_{\mathrm{P}_{x,R}^{\mathrm{BA}}}$, $M_{\mathrm{P}_{x,R}^{\mathrm{AA}}}$, and $M_{\mathrm{P}_{x,R}^{\mathrm{BB}}}$) of the polymer species ($\mathrm{P}_{x,R}^{\mathrm{BA}}$, $\mathrm{P}_{x,R}^{\mathrm{AA}}$, and $\mathrm{P}_{x,R}^{\mathrm{BB}}$); see their chemical structures in Table 2:

$$M_{\mathrm{P}_{x,R}^{\mathrm{BA}}} = x\,\mathrm{M}_{\mathrm{MDI}} + R\,M_r + x\,\mathrm{M}_{\mathrm{H_2O}} \qquad (x,R=1,2,...) \quad \text{(A.1)}$$

$$M_{\mathrm{P}_{x,R}^{\mathrm{AA}}} = (x+1)\,\mathrm{M}_{\mathrm{MDI}} + R\,M_r + x\,\mathrm{M}_{\mathrm{H_2O}} \qquad (x,R=1,2,...) \quad \text{(A.2)}$$

$$M_{\mathrm{P}_{x,R}^{\mathrm{BB}}} = (x-1)\,\mathrm{M}_{\mathrm{MDI}} + R\,M_r + x\,\mathrm{M}_{\mathrm{H_2O}} \qquad (x,R=1,2,...) \quad \text{(A.3)}$$

where $\mathrm{M}_{\mathrm{MDI}}$ (= 250.25 g mol^{-1}) is the molar mass of MDI; $\mathrm{M}_{\mathrm{H_2O}}$ (= 18 g mol^{-1}) is the molar mass of the –OH and –H end groups in PTMO; and M_r (= 72 g mol^{-1}) is the molar mass of a PTMO repeating unit.

The following expressions were used to calculate the average molar masses of the total polymer.

$$\bar{M}_{\mathrm{n,P}}(t) = \frac{\sum_{\forall x}\sum_{\forall R}\left\{\left[\mathrm{P}_{x,R}^{\mathrm{AA}}\right](t)\times M_{\mathrm{P}_{x,R}^{\mathrm{AA}}}\right\} + \sum_{\forall x}\sum_{\forall R}\left\{\left[\mathrm{P}_{x,R}^{\mathrm{BA}}\right](t)\times M_{\mathrm{P}_{x,R}^{\mathrm{BA}}}\right\} + \sum_{\forall x}\sum_{\forall R}\left\{\left[\mathrm{P}_{x,R}^{\mathrm{BB}}\right](t)\times M_{\mathrm{P}_{x,R}^{\mathrm{BB}}}\right\}}{\sum_{\forall x}\sum_{\forall R}\left[\mathrm{P}_{x,R}^{\mathrm{AA}}\right](t) + \sum_{\forall x}\sum_{\forall R}\left[\mathrm{P}_{x,R}^{\mathrm{BA}}\right](t) + \sum_{\forall x}\sum_{\forall R}\left[\mathrm{P}_{x,R}^{\mathrm{BB}}\right](t)} \qquad \text{(A.4)}$$

$$(x,R=1,2,...)$$

$$\bar{M}_{\mathrm{w,P}}(t) = \frac{\sum_{\forall x}\sum_{\forall R}\left\{c_{\mathrm{P}_{x,R}^{\mathrm{AA}}}(t)\times M_{\mathrm{P}_{x,R}^{\mathrm{AA}}}\right\} + \sum_{\forall x}\sum_{\forall R}\left\{c_{\mathrm{P}_{x,R}^{\mathrm{BA}}}(t)\times M_{\mathrm{P}_{x,R}^{\mathrm{BA}}}\right\} + \sum_{\forall x}\sum_{\forall R}\left\{c_{\mathrm{P}_{x,R}^{\mathrm{BB}}}(t)\times M_{\mathrm{P}_{x,R}^{\mathrm{BB}}}\right\}}{\sum_{\forall x}\sum_{\forall R}c_{\mathrm{P}_{x,R}^{\mathrm{AA}}}(t) + \sum_{\forall x}\sum_{\forall R}c_{\mathrm{P}_{x,R}^{\mathrm{BA}}}(t) + \sum_{\forall x}\sum_{\forall R}c_{\mathrm{P}_{x,R}^{\mathrm{BB}}}(t)} \qquad \text{(A.5)}$$

$$(x,R=1,2,...)$$

Similarly, for the global reaction mixture that includes MDI, one has:

$$\bar{M}_{\mathrm{n,G}}(t) = \frac{\left[\mathrm{MDI}^{\mathrm{AA}}\right](t)\times\mathrm{M}_{\mathrm{MDI}} + \sum_{\forall x}\sum_{\forall R}\left\{\left[\mathrm{P}_{x,R}^{\mathrm{AA}}\right](t)\times M_{\mathrm{P}_{x,R}^{\mathrm{AA}}}\right\} + \sum_{\forall x}\sum_{\forall R}\left\{\left[\mathrm{P}_{x,R}^{\mathrm{BA}}\right](t)\times M_{\mathrm{P}_{x,R}^{\mathrm{BA}}}\right\} + \sum_{\forall x}\sum_{\forall R}\left\{\left[\mathrm{P}_{x,R}^{\mathrm{BB}}\right](t)\times M_{\mathrm{P}_{x,R}^{\mathrm{BB}}}\right\}}{\left[\mathrm{MDI}^{\mathrm{AA}}\right](t) + \sum_{\forall x}\sum_{\forall R}\left[\mathrm{P}_{x,R}^{\mathrm{AA}}\right](t) + \sum_{\forall x}\sum_{\forall R}\left[\mathrm{P}_{x,R}^{\mathrm{BA}}\right](t) + \sum_{\forall x}\sum_{\forall R}\left[\mathrm{P}_{x,R}^{\mathrm{BB}}\right](t)}$$

$$(x,R=1,2,...)$$

(A.6)

$$\bar{M}_{\mathrm{w,G}}(t)=\frac{c_{\mathrm{MDI^{AA}}}(t)\times \mathrm{M_{MDI}}+\sum_{\forall x}\sum_{\forall R}\left\{c_{\mathrm{P}_{x,R}^{\mathrm{AA}}}(t)\times M_{\mathrm{P}_{x,R}^{\mathrm{AA}}}\right\}+\sum_{\forall x}\sum_{\forall R}\left\{c_{\mathrm{P}_{x,R}^{\mathrm{BA}}}(t)\times M_{\mathrm{P}_{x,R}^{\mathrm{BA}}}\right\}+\sum_{\forall x}\sum_{\forall R}\left\{c_{\mathrm{P}_{x,R}^{\mathrm{BB}}}(t)\times M_{\mathrm{P}_{x,R}^{\mathrm{BB}}}\right\}}{c_{\mathrm{MDI^{AA}}}(t)+\sum_{\forall x}\sum_{\forall R}c_{\mathrm{P}_{x,R}^{\mathrm{AA}}}(t)+\sum_{\forall x}\sum_{\forall R}c_{\mathrm{P}_{x,R}^{\mathrm{BA}}}(t)+\sum_{\forall x}\sum_{\forall R}c_{\mathrm{P}_{x,R}^{\mathrm{BB}}}(t)} \quad (A.7)$$

$$(x,R=1,2,...)$$

The moles of unreacted end groups ($n_{\mathrm{-NCO}}$ and $n_{\mathrm{-OH}}$), and the moles of generated urethane groups ($n_{\mathrm{-NHCOO-}}$) were obtained through (see Table 2):

$$n_{\mathrm{-NCO}}(t)=2\,n_{\mathrm{MDI^{AA}}}(t)+2\sum_{\forall x}\sum_{\forall R}n_{\mathrm{P}_{x,R}^{\mathrm{AA}}}(t)+\sum_{\forall x}\sum_{\forall R}n_{\mathrm{P}_{x,R}^{\mathrm{BA}}}(t) \qquad (x,R=1,2,...) \quad (A.8)$$

$$n_{\mathrm{-OH}}(t)=2\sum_{\forall x}\sum_{\forall R}n_{\mathrm{P}_{x,R}^{\mathrm{BB}}}(t)+\sum_{\forall x}\sum_{\forall R}n_{\mathrm{P}_{x,R}^{\mathrm{BA}}}(t) \qquad (x,R=1,2,...) \quad (A.9)$$

$$n_{\mathrm{-NHCOO-}}(t)=\sum_{\forall x}\sum_{\forall R}\left\{(2x)\times n_{\mathrm{P}_{x,R}^{\mathrm{AA}}}(t)\right\}+\sum_{\forall x}\sum_{\forall R}\left\{(2x-1)\times n_{\mathrm{P}_{x,R}^{\mathrm{BA}}}(t)\right\}+\sum_{\forall x}\sum_{\forall R}\left\{(2x-2)\times n_{\mathrm{P}_{x,R}^{\mathrm{BB}}}(t)\right\} \qquad (x,R=1,2,...) \quad (A.10)$$

Finally, the total molar concentrations of unreacted end groups ([–NCO] and [–OH]), and of generated urethane groups ([–NHCOO–]) are given by (see Table 2):

$$\left[-\mathrm{NCO}\right](t)=2\left[\mathrm{MDI^{AA}}\right](t)+2\sum_{\forall x}\sum_{\forall R}\left[\mathrm{P}_{x,R}^{\mathrm{AA}}\right](t)+\sum_{\forall x}\sum_{\forall R}\left[\mathrm{P}_{x,R}^{\mathrm{BA}}\right](t) \qquad (x,R=1,2,...) \quad (A.11)$$

$$\left[-\mathrm{OH}\right](t)=2\sum_{\forall x}\sum_{\forall R}\left[\mathrm{P}_{x,R}^{\mathrm{BB}}\right](t)+\sum_{\forall x}\sum_{\forall R}\left[\mathrm{P}_{x,R}^{\mathrm{BA}}\right](t) \qquad (x,R=1,2,...) \quad (A.12)$$

$$\left[-\mathrm{NHCOO}-\right](t)=\sum_{\forall x}\sum_{\forall R}\left\{(2x)\times\left[\mathrm{P}_{x,R}^{\mathrm{AA}}\right](t)\right\}+\sum_{\forall x}\sum_{\forall R}\left\{(2x-1)\times\left[\mathrm{P}_{x,R}^{\mathrm{BA}}\right](t)\right\}+\sum_{\forall x}\sum_{\forall R}\left\{(2x-2)\times\left[\mathrm{P}_{x,R}^{\mathrm{BB}}\right](t)\right\} \qquad (x,R=1,2,...) \quad (A.13)$$

APPENDIX B: MASS BALANCE OF THE SINGLE-PHASE MODEL

From the reaction mechanism of Eqs (4.1)-(4.6) in Table 4, the following mass balances are derived for the unreacted MDI and evolving polymer species $P_{x,R}^{BA}$, $P_{x,R}^{AA}$, and $P_{x,R}^{BB}$. In the right-hand side of Eqs (B.1)-(B.4), the factors (1, 2, or 4) quantify the reaction probabilities between reacting species.

$$\frac{d\left[MDI^{AA}\right](t)}{dt} = -4k_1\left[MDI^{AA}\right](t)\times\sum_{\forall x}\sum_{\forall R}\left[P_{x,R}^{BB}\right](t) - 2k_1\left[MDI^{AA}\right](t)\times\sum_{\forall x}\sum_{\forall R}\left[P_{x,R}^{BA}\right](t) \tag{B.1}$$

$$\begin{aligned}\frac{d\left[P_{x,R}^{BA}\right](t)}{dt} &= 4k_1\left[MDI^{AA}\right](t)\times\left[P_{x,R}^{BB}\right](t) + k_1\sum_{x_1=1}^{x}\sum_{R_1=1}^{R}\left\{\left[P_{x_1,R_1}^{BA}\right](t)\times\left[P_{(x-x_1),(R-R_1)}^{BA}\right](t)\right\} + \\ &+ 4k_1\sum_{x_1=1}^{x}\sum_{R_1=1}^{R}\left\{\left[P_{x_1,R_1}^{AA}\right](t)\times\left[P_{(x-x_1),(R-R_1)}^{BB}\right](t)\right\} - \\ &- 2k_1\left[P_{x,R}^{BA}\right](t)\times\left[MDI^{AA}\right](t) - 2k_1\left[P_{x,R}^{BA}\right](t)\times\sum_{\forall x}\sum_{\forall R}\left[P_{x,R}^{BA}\right](t) - \\ &- 2k_1\left[P_{x,R}^{BA}\right](t)\times\sum_{\forall x}\sum_{\forall R}\left[P_{x,R}^{AA}\right](t) - 2k_1\left[P_{x,R}^{BA}\right](t)\times\sum_{\forall x}\sum_{\forall R}\left[P_{x,R}^{BB}\right](t) \\ &\left(x, R = 1, 2, ...\right)\end{aligned} \tag{B.2}$$

$$\begin{aligned}\frac{d\left[P_{x,R}^{AA}\right](t)}{dt} &= 2k_1\left[MDI^{AA}\right](t)\times\left[P_{x,R}^{BA}\right](t) + 2k_1\sum_{x_1=1}^{x}\sum_{R_1=1}^{R}\left\{\left[P_{x_1,R_1}^{BA}\right](t)\times\left[P_{(x-x_1),(R-R_1)}^{AA}\right](t)\right\} - \\ &- 2k_1\left[P_{x,R}^{AA}\right](t)\times\sum_{\forall x}\sum_{\forall R}\left[P_{x,R}^{BA}\right](t) - 4k_1\left[P_{x,R}^{AA}\right](t)\times\sum_{\forall x}\sum_{\forall R}\left[P_{x,R}^{BB}\right](t) \\ &\left(x, R = 1, 2, ...\right)\end{aligned} \tag{B.3}$$

$$\begin{aligned}\frac{d\left[P_{x,R}^{BB}\right](t)}{dt} &= 2k_1\sum_{x_1=1}^{x}\sum_{R_1=1}^{R}\left\{\left[P_{x_1,R_1}^{BA}\right](t)\times\left[P_{(x-x_1),(R-R_1)}^{BB}\right](t)\right\} - \\ &- 4k_1\left[P_{x,R}^{BB}\right](t)\times\left[MDI^{AA}\right](t) - 2k_1\left[P_{x,R}^{BB}\right](t)\times\sum_{\forall x}\sum_{\forall R}\left[P_{x,R}^{BA}\right](t) - \\ &- 4k_1\left[P_{x,R}^{BB}\right](t)\times\sum_{\forall x}\sum_{\forall R}\left[P_{x,R}^{AA}\right](t) \\ &\left(x, R = 1, 2, ...\right)\end{aligned} \tag{B.4}$$

APPENDIX C

To prove that the total $\bar{M}_{n,G}(p)$ remains unaffected by the split of reagents, its expression of Eq. (13a) may be recuperated by application of the following analytical procedure: i) obtain expressions for $\bar{M}^{0}_{n,G,1}$ and $\bar{M}^{0}_{n,G,2}$ by applying Eq. (13c) onto phases 1 and 2 with ($n^{0}_{-OH,1}$, $n^{0}_{-NCO,1}$) and ($n^{0}_{-OH,2}$, $n^{0}_{-NCO,2}$), respectively; ii) obtain expressions for $\bar{M}_{n,G,1}(p)$ and $\bar{M}_{n,G,2}(p)$ by applying Eq. (13a) onto phases 1 and 2 with (r'_1, p_1, $\bar{M}^{0}_{n,G,1}$) and (r'_2, p_2, $\bar{M}^{0}_{n,G,2}$), respectively; iii) replace the results of item i) and Eqs (15b) and (17a) into the results of item ii); and finally iv) replace the obtained expressions for $\bar{M}_{n,G,1}(p)$ and $\bar{M}_{n,G,2}(p)$ into:

$$\bar{M}_{n,G} = \frac{n^{0}_{-OH,1} + n^{0}_{-NCO,1}}{n^{0}_{-OH} + n^{0}_{-NCO}} \times \bar{M}_{n,G,1} + \frac{n^{0}_{-OH,2} + n^{0}_{-NCO,2}}{n^{0}_{-OH} + n^{0}_{-NCO}} \times \bar{M}_{n,G,2} \tag{C.1}$$

REFERENCES

1 Polo, M. L.; Spontón, M. E.; Jaramillo, F.; Estenoz, D. A.; Meira, G. R. *J. Appl. Polym. Sci.* **2017**, *135*, 45747.

2 Król, P. In *Linear polyurethanes: synthesis methods, chemical structures, properties and applications*; VSP: Leiden, **2008**.

3 Lunardon, G.; Sumida, Y.; Vogl, O. *Angew. Makromol. Chemie* **1980**, *87* (1), 1–33.

4 Abouzahr, S.; Wilkes, G. L. *J. Appl. Polym. Sci.* **1984**, *29* (9), 2695–2711.

5 Miller, J. A.; Lin, S. B.; Hwang, K. K. S.; Wu, K. S.; Gibson, P. E.; Cooper, S. L. *Macromolecules* **1985**, *18* (1), 32–44.

6 Dušek, K.; Špirková, M.; Havliček, I. *Macromolecules* **1990**, *23* (6), 1774–1781.

7 Król, P.; Atamanczuk, B.; Plelichowskl, J. *J. Appl. Polym. Sci.* **1992**, *46* (12), 2139–2146.

8 Heintz, A. M.; Duffy, D. J.; Hsu, S. L.; Suen, W.; Chu, W.; Paul, C. W. *Macromolecules* **2003**, *36*, 2695–2704.

9 Ketata, N.; Sanglar, C.; Waton, H.; Alamercery, S.; Delolme, F.; Paisse, O.; Raffin, G.; Grenier-Loustalot, M. F. F. *Polym. Polym. Compos.* **2004**, *12* (8), 645–665.

10 Kothandaraman, H.; Nasar, A. S. *J. Macromol. Sci. Part A Pure Appl. Chem.* **1994**, *31* (3), 339–350.

11 Taylor, P.; Rochery, M.; Vroman, I.; Lam, T. M. *J. Macromol. Sci. Part A Pure Appl. Chem.* **2000**, *A37* (3), 259–275.

12 Grepinet, B.; Pla, F.; Hobbes, P. H.; Swaels, P. H.; Monge, T. H. *J. Appl. Polym. Sci.* **2000**, *75* (5), 705–712.

13 Grepinet, B.; Pla, F.; Hobbes, P.; Monge, T.; Swaels, P. *J. Appl. Polym. Sci.* **2001**, *81* (13), 3149–3160.

14 Król, P. *J. Appl. Polym. Sci.* **1995**, *57*, 739–749.

15 Chang, M.-C.; Chen, S.-A. *J. Polym. Sci. Part A Polym. Chem.* **1987**, *25* (9), 2543–2559.

16 Yang, P. F.; Han, Y. De; Li, T. D.; Li, J. Y. *Polym. Polym. Compos.* **2012**, *123*, 580–584.

17 Monaghan, S.; Pethrick, R. a. *Macromolecules* **2012**, *45* (9), 3928–3938.

18 Castro, J. M.; Lopez-Serrano, F.; Camargo, R. E.; Macosko, C. W.; Tirrell, M. *J. Appl. Polym. Sci.* **1981**, *26* (6), 2067–2076.

19 Hager, S. L.; MacRury, T. B.; Gerkin, R. M.; Critchfield, F. E. In *Urethane Chemistry and Applications*; K. N. Edwards, W. F. Gum, J. E. Johnson, F. E. Bailey, Jr., R. S. Graff, W. G. Glasser, D. K., Frisch, K. C., Eds.; American Chemical Society, **1981**; 149–166.

20 Camargo, R. E.; Macosko, C. W.; Tirrell, M.; Wellinghoff, S. T. *Polymer*. **1985**, *26* (8), 1145–1154.

21 Xu, M.; MacKnight, W. J.; Chen, C. H. Y.; Thomas, E. L. *Polymer*. **1983**, *24*, 1327–1332.

22 Chen, C. H. Y.; Briber, R. M.; Thomas, E. L.; Xu, M.; MacKnight, W. J. *Polymer*. **1983**, *24* (10), 1333–1340.

23 Sun, X.-D.; Sung, C. S. P. *Macromolecules* **1996**, *29* (9), 3198–3202.

24 Eceiza, A.; de la Caba, K.; Kortaberria, G.; Gabilondo, N.; Marieta, C.; Corcuera, M. A.; Mondragon, I. *Eur. Polym. J.* **2005**, *41* (12), 3051–3059.

25 Flory, P. J. *J. Am. Chem. Soc.* **1936**, *58* (7), 1877–1885.

26 Nanda, V. S.; Jain, S. C. *J. Chem. Phys.* **1968**, *49* (3), 1318–1320.

27 Miller, D. R.; Macosko, C. W. *Macromolecules* **1978**, *2* (9), 656–662.

28 Miller, D. R.; Macosko, C. W. *Macromolecules* **1980**, *13*, 1063–1069.

29 Gupta, S. K.; Kumar, A.; Bhargava, A. *Polymer*. **1979**, *20* (3), 305–310.

30 Gupta, S. K.; Kumar, A. In *Reaction Engineering of Step Growth Polymerization*; Luss, D.,

Ed.; Plenum Press: New York, **1987**.

31 Kuchanov, S.; Slot, H.; Stroeks, A. *Prog. Polym. Sci.* **2004**, *29* (6), 563–633.

32 Odian, G. In *Principles of Polymerization*; Odian, G., Ed.; John Wiley & Sons, Inc.: New York, **2004**; Chapter 2, 39–197.

33 Costa, M. R. P. F. N.; Bachmann, R. In *Handbook of Polymer Reaction Engineering*; Meyer, T., Keurentjes, J., Eds.; Wiley-VCH Verlag GmbH & Co.: Weinheim, Germany, **2005**; Chapter 3, 57–151.

34 Sarmoria, C.; Vallés, E. M.; Miller, D. R. *Macromolecules* **1990**, *23* (2), 580–589.

35 Seavey, K. C.; Liu, Y. A. In *Step-Growth Polymerization Process Modeling and Product Design*; John Wiley & Sons, Inc.: Hoboken, New Jersey, **2008**; Chapter 5, 135–197.

36 Choi, K. Y.; McAuley, K. B. In *Polymer Reaction Engineering*; Asúa, J. M., Ed.; Blackwell Publishing Ltd: Oxford, UK, **2008**; Chapter 7, 273–314.

37 Zhu, S.; Hamielec, A. In *Polymer Science: A Comprehensive Reference*; Elsevier B.V., **2012**; Vol. 4, Chapter 4.32, 779–831.

38 Elizalde, L. E.; Santos-Villareal, G. de los; Santigao-García, J. L.; Aguilar-Vega, M. In *Handbook of Polymer Synthesis, Characterization, and Processing*; Saldívar-Guerra, E., Vivaldo-Lima, E., Eds.; John Wiley & Sons, Inc.: Hoboken, New Jersey, **2013**; Chapter 3, 43–63.

39 Gandhi, K. S.; Babu, S. V. *AIChE J.* **1979**, *25* (2), 266–272.

40 Gandhi, K. S.; Babu, S. V. *Macromolecules* **1980**, *13*, 791–798.

41 Król, P.; Gawdzik, A. *J. Appl. Polym. Sci.* **1995**, *58*, 729–743.

42 Król, P. *J. Appl. Polym. Sci.* **1996**, *61*, 2207–2219.

43 Król, P. *J. Appl. Polym. Sci.* **1998**, *69*, 169–181.

44 Król, P.; Galina, H.; Kaczmarski, K. *Macromol. Theory Simulations* **1999**, *8*, 129–136.

45 Case, L. C. *J. Polym. Sci.* **1958**, *29*, 455–495.

46 Peebles, L. H. J. *Macromolecules* **1974**, *7*, 872–882.

47 Peebles, L. H. J. *Macromolecules* **1976**, *9*, 58–61.

48 Lopez-Serrano, F.; Castro, J. M.; Macosko, C. W.; Tirrell, M. *Polymer* **1980**, *21* (3), 263–273.

49 Johnson, A. F.; O'Driscoll, K. F. *Eur. Polym. J.* **1984**, *20* (10), 979–983.

50 Speckhard, T. A.; Miller, J. A.; Cooper, S. L. *Macromolecules* **1986**, *19* (6), 1558–1567.

51 Miller, J. A.; Speckhard, T. A.; Cooper, S. L. *Macromolecules* **1986**, *19*, 1568–1574.

52 Miller, J. A.; Speckhard, T. A.; Homan, J. G.; Cooper, S. L. *Polymer.* **1987**, *28* (5), 758–767.

53 Speckhard, T. A.; Homan, J. G.; Miller, J. A.; Coopert, S. L. *Polymer.* **1987**, *28*, 768–776.

54 Shiau, L. D. *Macromol. Theory Simulations* **2001**, *10* (3), 179–186.

Table 1. Main characteristics of the publications that contain mathematical models for synthesis of linear polyurethanes. our contributions are in the last two columns.

		Gandhi and Babu (1979) [39]	Gandhi and Babu (1980) [40]	Król and Gawzdik (1995) [41]	Król (1996) [42]	Król (1998) [43]	Król et al. (1999) [44]	Grepinet et al. (2001) [13]	Case (1958) [45]	Peebles (1974) [46]	Peebles (1976) [47]	Lopez-Serrano et al. (1980) [48]	Johnson and O'Driscoll (1984) [49]	Speckhard et al. (1986) [50]	Miller et al. (1986) [51]	Miller et al. (1987) [52]	Specckhard et al. (1987) [53]	Shiau (2001) [54]	Polo et al. I (2017) [1]	Polo et al. II (This Work)
Synthesis of:	i) Oligomers (One-Step Stoichiometric Reaction at Low Conversion)	X[a]	X[a]	X[b]	X[b]	X[b]	X[b]													
	ii) Oligomers (Non-Stoichiometric Prepolymerization at High Conversion)	X[a]	X[a]					X[c]											X[g]	X[g]
	iii) High Polymers (Stoichiometric Finishing at High Conversion)									X[e]	X[e]			X[e]					X[h]	
	iv) High Polymers (One-Step Stoichiometric at High Conversion)								X[d]		X[d]	X[d]	X[d]	X[d]	X[d]	X[d]	X[f]	X[d]		
Model Type	Stochastic	X	X					X	X	X	X	X	X	X	X	X	X	X		
	Deterministic			X	X	X	X												X	X
Model Assumptions	"Classical" Equal Reactivity			X					X	X			X	X	X		X	X	X	X
	Different Reactivities of –NCO Groups in Diisocyanate	X	X			X	X	X		X	X		X	X						
	Different Reactivities of –OH Groups in Macrodiol and in Chain Extender											X	X			X	X			
	Rate Constant Depends on Molar Mass				X															
Reaction Phases	Single-Phase Homogeneous	X	X	X	X	X	X	X	X	X	X	X	X	X			X	X	X	X
	Double-Phases (with Each Phase Homogenous)														X	X	X			X
Model Predictions	Concentration of End and Internal Urethane Groups							X											X*	X*
	Number Average Number of Structural Units									X	X	X	X						X*	X*
	Chain Length Distribution								X				X							X
	Number-Average Molar Mass	X	X	X*	X*	X	X		X	X	X	X		X	X	X	X*	X		X*
	Molar Mass Distribution and/or Weight Average Molar Mass	X	X	X*	X*	X*	X*	X*	X			X		X	X	X	X*	X		X*
	Chemical Composition Distribution													X	X	X				X
	Hard-Segments Distribution									X	X					X				

[a] Generic diisocyanate + low molar mass diol. [b] 2,4-TDI and BD. [c] 2,4-TDI, 2,6-TDI and PPG. [d] Generic diisocyanate + macrodiol + chain extender. [e] Generic addition of a chain extender to the product of a non-stoichiometric Prepolymerization between a diisocyanate and a macrodiol. [f] 2,4-TDI or 2,6-TDI, HTPB, and BD. [g] MDI and PTMO. [h] Addition of BD to the product of a non-stoichiometric Prepolymerization between MDI and PTMO. * Verified with experimental data.

TABLE 2. Global Prepolymerization scheme, and employed nomenclature. Along the reaction, the polymer species exhibit all the three combinations of end groups. But at the reaction end, the mixture only contains isocyanate-capped oligomers and unreacted MDI.

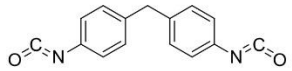	MDI^{AA}	
+	+	
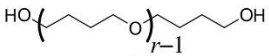	$P^{BB}_{1,R}$	$(R = r = 1, 2, ...)$
	k_1	
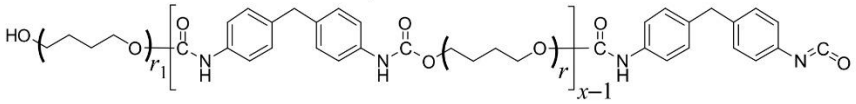	$P^{BA}_{x,R}$	$(x = 1, 2, ...)$ $(r, r_1 = 1, 2, ...)$ $(R = r_2 + \sum_{\forall r} r)$
+	+	
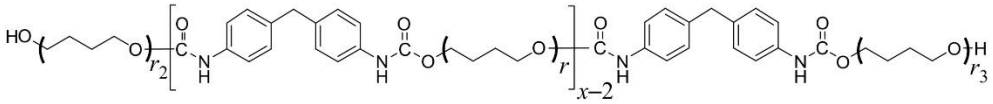	$P^{BB}_{x,R}$	$(x = 2, 3, ...)$ $(r, r_2, r_3 = 1, 2, ...)$ $(R = r_2 + \sum_{\forall r} r + r_3)$
+	+	
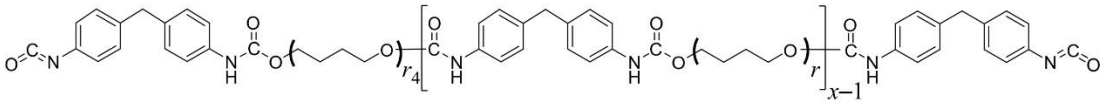	$P^{AA}_{x,R}$	$(x = 1, 2, ...)$ $(r, r_4 = 1, 2, ...)$ $(R = r_4 + \sum_{\forall r} r)$

TABLE 3. Experiments 1-5. Upper sections: recipes and final average molar masses, taken from Polo et al.[1] Lower sections: simulation results by: a) the single-phase model with ($k_{1,I}$ = 0.00107 L mol^{-1} s^{-1}); and b) the double-phases model with ($\Delta r'_1/r'$ = 0.567), ($\Delta r'_2/r'$ = -0.643), and ($k_{1,II}$ = 0.00265 L mol^{-1} s^{-1}). Nomenclature: superscript 0: initial conditions; ω: weight fraction; subscript P: polymer; subscript G: global mixture; p: extent of reaction; subscripts 1 and 2: phases 1 and 2; X: molar fraction of –OH end groups.

		Exp. 1	Exp. 2	Exp. 3	Exp. 4	Exp. 5
Recipes and final reaction times						
$r' = n^0_{PTMO}/n^0_{MDI}$ [Eq. (13b)]	(—)	0.3	0.7	0.3	0.7	0.5
$n^0_{PTMO,1}$ or $n^0_{PTMO,2}$	(mol)	0.00182 [a, c]	0.00280 [a]	0.00201 [b]	0.00208 [b]	0.00335 [a]
n^0_{MDI}	(mol)	0.00605 [c]	0.00400	0.0067	0.00297	0.0067
Mass of MDI	(g)	1.517	1.001	1.677	0.743	1.677
ω^0_{MDI}	(—)	0.488	0.264	0.292	0.150	0.334
$\boldsymbol{t_{end}}$	(min.)	**30**	30	60	30	30
Measurements at t_{end}						
$\bar{M}_{n,P}(t_{end})$	(g mol^{-1})	1690	4470	3310	3220	2620
$\boldsymbol{\bar{M}_{w,P}(t_{end})}$	(g mol^{-1})	**3540**	11100	10900	7430	5340
$\bar{M}_{w,P}/\bar{M}_{n,P}(t_{end})$	(—)	2.09	2.48	3.29	2.31	2.04
$\omega_{MDI}(t_{end})$	(—)	0.186	0.105	0.094	0.060	0.061
$\bar{M}_{n,G}(t_{end})$	(g mol^{-1})	820	2380	1540	1880	1660
$\bar{M}_{w,G}(t_{end})$	(g mol^{-1})	2930	9960	9900	7000	5030
$\bar{M}_{w,G}/\bar{M}_{n,G}(t_{end})$	(—)	3.57	4.18	6.43	3.72	3.03
a) Predictions by the single-phase model						
$p(t_{end})$	(—)	0.997	0.914	0.999	0.777	0.975
$\bar{M}_{n,P}(t_{end})$	(g mol^{-1})	1850	2840	3600	4110	2360
$\bar{M}_{w,P}(t_{end})$	(g mol^{-1})	2800	4910	6500	7870	3830
$\bar{M}_{w,P}/\bar{M}_{n,P}(t_{end})$	(—)	1.51	1.73	1.81	1.91	1.63
$\omega_{MDI}(t_{end})$	(—)	0.239	0.038	0.139	0.030	0.099
$\boldsymbol{\bar{M}_{n,G}(t_{end})}$	(g mol^{-1})	**733**	2040	1260	2790	1310
$\bar{M}_{w,G}(t_{end})$	(g mol^{-1})	2190	4740	5630	7630	3490
$\bar{M}_{w,G}/\bar{M}_{n,G}(t_{end})$	(—)	3.00	2.58	4.47	2.73	2.66
b) Predictions by the double-phases model						
r'_1, r'_2	(—)	0.130; 0.494	0.436; 1.00	0.130; 0.493	0.436; 1.00	0.216; 0.822
$X^0_{-OH,1}$; $X^0_{-OH,2}$	(—)	0.115; 0.330	0.303; 0.500	0.115; 0.330	0.303; 0.500	0.178; 0.451
ω_1; ω_2	(—)	0.377; 0.623	0.389; 0.611	0.316; 0.684	0.360; 0.640	0.340; 0.660
$p_1(t_{end})$; $p_2(t_{end})$	(—)	0.999; 0.995	0.983; 0.845	0.999; 0.998	0.894; 0.733	0.998; 0.931
$p(t_{end})$	(—)	0.997	0.891	0.998	0.786	0.946
$\bar{M}_{n,P}(t_{end})$	(g mol^{-1})	2150	3050	4220	4520	2980
$\bar{M}_{n,P,1}(t_{end})$; $\bar{M}_{n,P,2}(t_{end})$	(g mol^{-1})	1550; 2450	2180; 3920	2950; 4860	3780; 5030	1690; 4030
$\boldsymbol{\bar{M}_{w,P}(t_{end})}$	(g mol^{-1})	**3540**	5970	8110	8900	6090
$\bar{M}_{w,P,1}(t_{end})$; $\bar{M}_{w,P,2}(t_{end})$	(g mol^{-1})	2200; 3970	3460; 7370	5200; 9000	6990; 9900	2470; 7320
$\bar{M}_{w,P}/\bar{M}_{n,P}(t_{end})$	(—)	1.65	1.96	1.92	1.97	2.04
$\omega_{MDI}(t_{end})$	(—)	0.255	0.054	0.149	0.034	0.128
$\boldsymbol{\bar{M}_{n,G}(t_{end})}$	(g mol^{-1})	**733**	1910	1260	2870	1240
$\bar{M}_{w,G}(t_{end})$	(g mol^{-1})	2700	5660	6940	8610	5340
$\bar{M}_{w,G}/\bar{M}_{n,G}(t_{end})$	(—)	3.69	2.97	5.52	3.00	4.30

[a] $PTMO_1$. [b] $PTMO_2$. [c] *Ex-post* values, as readjusted in Ref.[1]

TABLE 4. Prepolymerization mechanism at polymer species level.

$MDI^{AA} + P^{BB}_{x,R} \xrightarrow{k_1} P^{BA}_{x,R}$	$(x, R = 1, 2, \ldots)$	(4.1)
$MDI^{AA} + P^{BA}_{x,R} \xrightarrow{k_1} P^{AA}_{x,R}$	$(x, R = 1, 2, \ldots)$	(4.2)
$P^{BA}_{x_1,R_1} + P^{AA}_{x_2,R_2} \xrightarrow{k_1} P^{AA}_{x_1+x_2,R_1+R_2}$	$(x_1, x_2, R_1, R_2 = 1, 2, \ldots)$	(4.3)
$P^{BA}_{x_1,R_1} + P^{BA}_{x_2,R_2} \xrightarrow{k_1} P^{BA}_{x_1+x_2,R_1+R_2}$	$(x_1, x_2, R_1, R_2 = 1, 2, \ldots)$	(4.4)
$P^{BA}_{x_1,R_1} + P^{BB}_{x_2,R_2} \xrightarrow{k_1} P^{BB}_{x_1+x_2,R_1+R_2}$	$(x_1, x_2, R_1, R_2 = 1, 2, \ldots)$	(4.5)
$P^{AA}_{x_1,R_1} + P^{BB}_{x_2,R_2} \xrightarrow{k_1} P^{AB}_{x_1+x_2,R_1+R_2}$	$(x_1, x_2, R_1, R_2 = 1, 2, \ldots)$	(4.6)

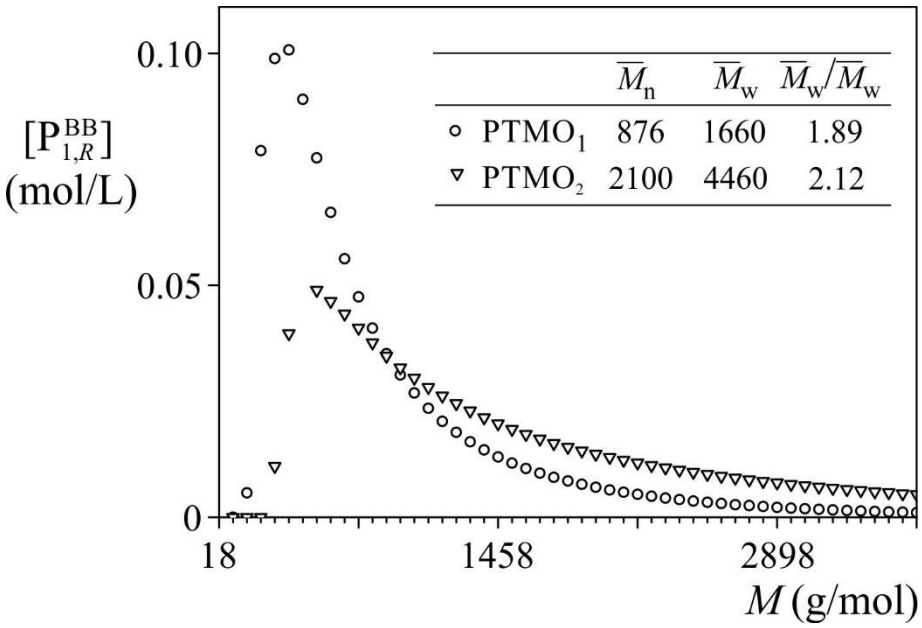

FIGURE 1. Discrete and normalized number MMDs of the two employed macrodiols ($PTMO_1$ and $PTMO_2$), with corresponding averages. The discrete points are defined at multiples of 72 g mol^{-1} (the molar mass of the PTMO repeating unit).

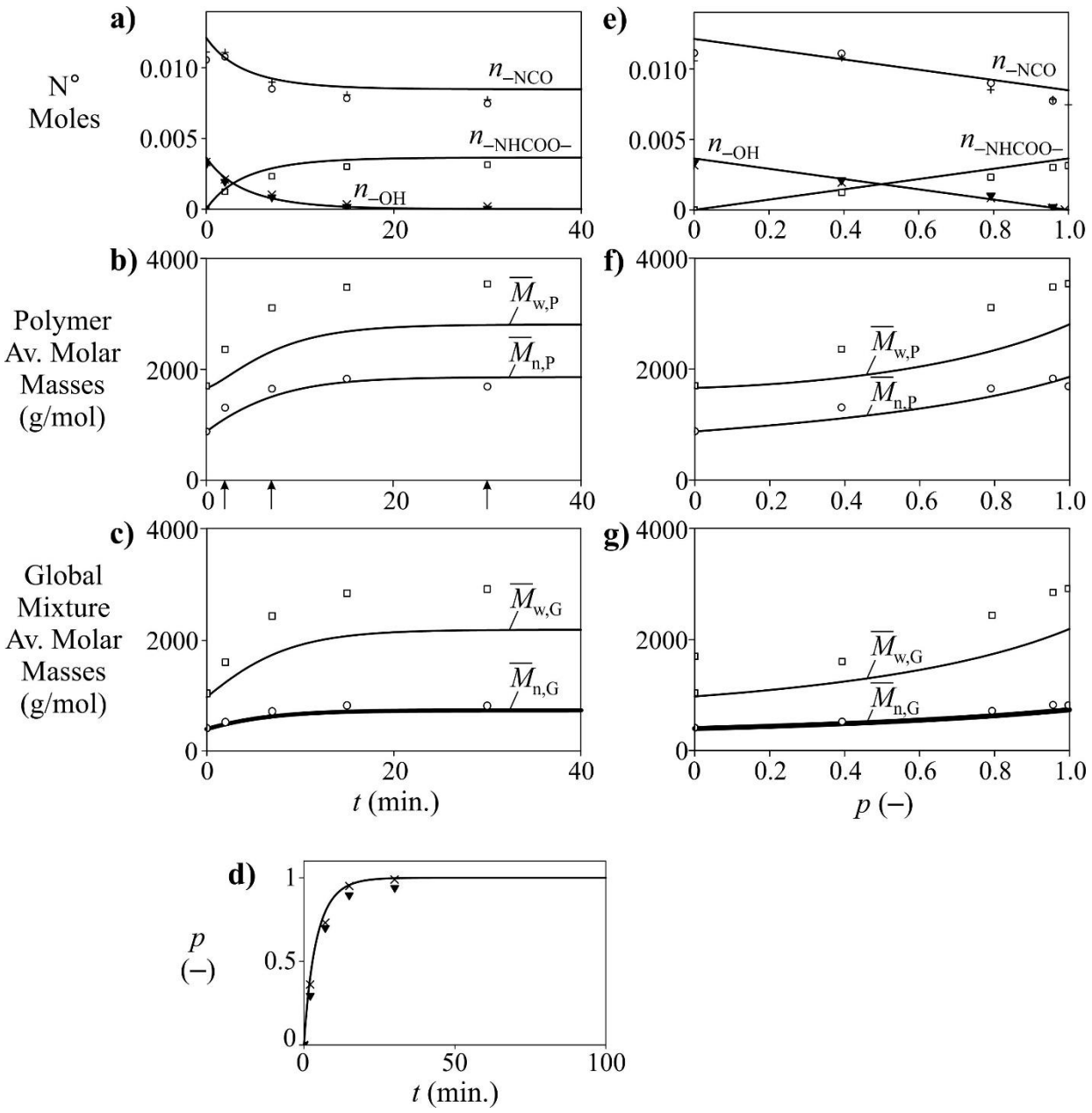

FIGURE 2. Experiment 1: measurements reproduced from Ref.[1] (in points) and predictions from the single-phase model (in continuous trace) with $k_{1,I}$ = 0.00107 L mol^{-1} s^{-1}. Figures 2a-d show the time evolutions of: a) number of moles of unreacted end groups (n_{-NCO} and n_{-OH}) and generated internal groups ($n_{-NHCCO-}$); b) average molar masses of the total polymer ($\overline{M}_{n,P}$, $\overline{M}_{w,P}$); c) average molar masses of the global reaction mixture ($\overline{M}_{n,G}$, $\overline{M}_{w,G}$); and d) the extents of reaction (p) estimated through Eqs (11). Figures 2e-g represent the same variables of Figures 2a-c, but *vs* the extent of reaction, transformed by the $p(t)$ function of Figure 2d.

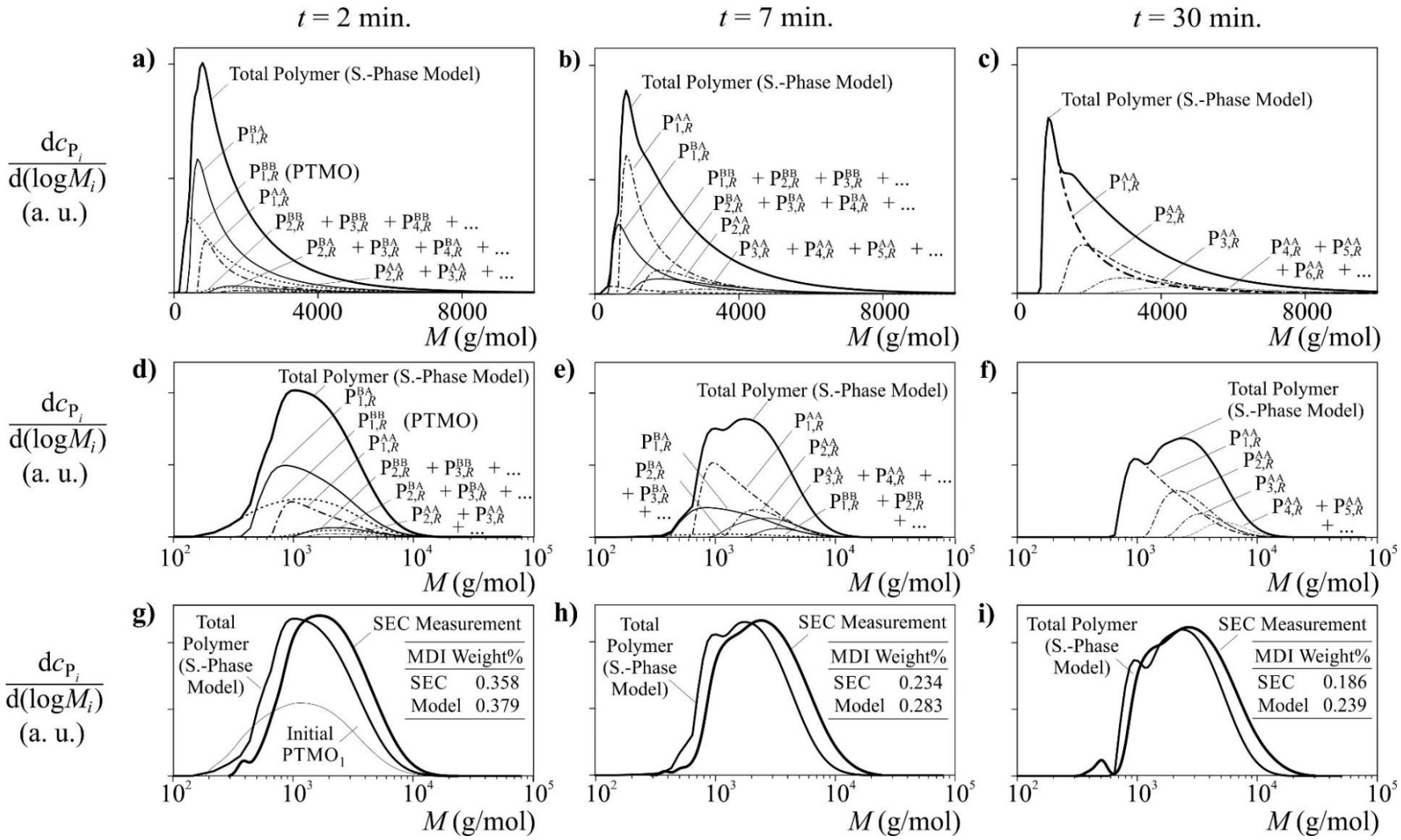

FIGURE 3. Experiment 1: Weight MMDs at t = 2, 7, and 30 min. a-c) Single-phase model predictions for the total polymer and main polymer topologies, with linear horizontal axes. d-f) *Idem* to figures a-c), but with logarithmic horizontal axes. g-i) SEC measurements and single-phase model predictions for the MMDs of the total polymer, showing the weight fractions of unreacted MDI.

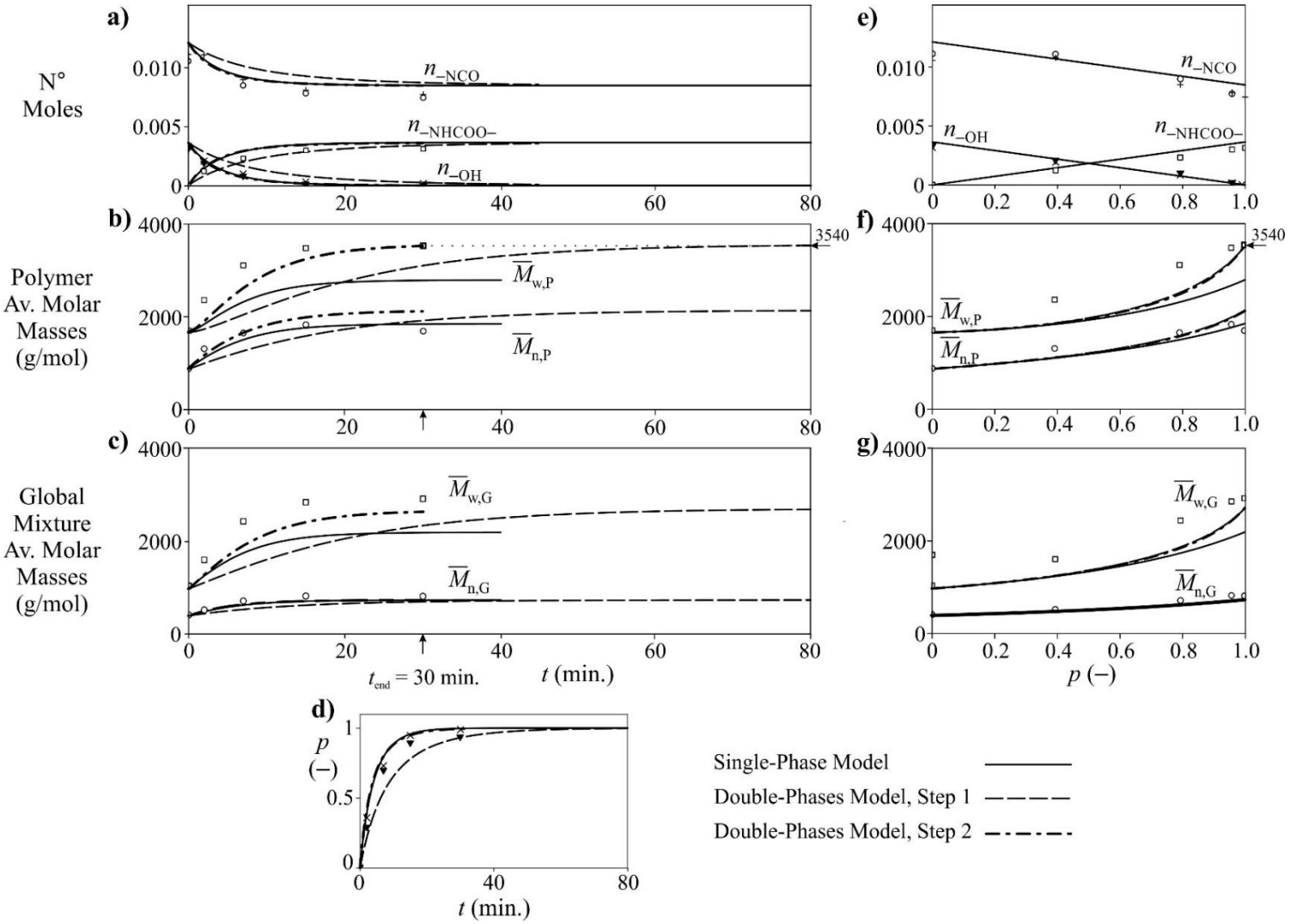

FIGURE 4. Adjustment of the double-phases model (in discontinuous trace) to the measurements of Exp. 1 (in points), and comparison with the results of the single-phase model (in continuous trace). In step 1, the split of reagents (r'_1 = 0.567, r'_2 = -0.643) reproduces the experimental value of $\overline{M}_{w,P}$ (= 3540 g mol^{-1}) at a high extent of reaction (Figure 4f), but not at t_{end} = 30 min. (Figure 4b). In step 2, the rate constant was increased into ($k_{1,II}$ = 0.00265 L mol^{-1} s^{-1}), in order to predict the experimental value of $\overline{M}_{w,P}$ at t_{end} = 30 min.

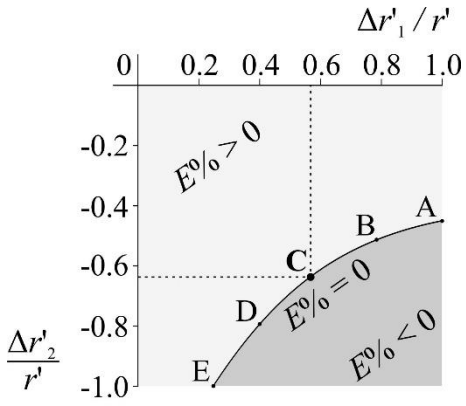

Point	r'_1	r'_2
A	0.000	0.436
B	0.065	0.455
C	**0.130**	**0.494**
D	0.180	0.539
E	0.226	0.600

FIGURE 5. Step 1 of the adjustment procedure of the double-phases model, applied to the measurements of Experiment 1: determination of the imbalances r'_1 and r'_2 in phases 1 and 2 that reproduce $\bar{M}_{w,P}$ = 3540 g mol^{-1} at a high extent of reaction. The figure shows the percentage of error (E%) [see Eq. (19)] for all the possible combinations of fractional variations of the global imbalances ($\Delta r'_1/r'$, $\Delta r'_2/r'$). The solutions with E% = 0 are represented by the curve shown in continuous line, while the grey zones are non zero solutions. The phase imbalances at points A to E are presented in the enclosed table. From all the possible solutions, point C was selected at ($\Delta r'_1/r'$ = 0.567, $\Delta r'_2/r'$ = -0.643), or equivalently with (r'_1 = 0.130, r'_2 = 0.494).

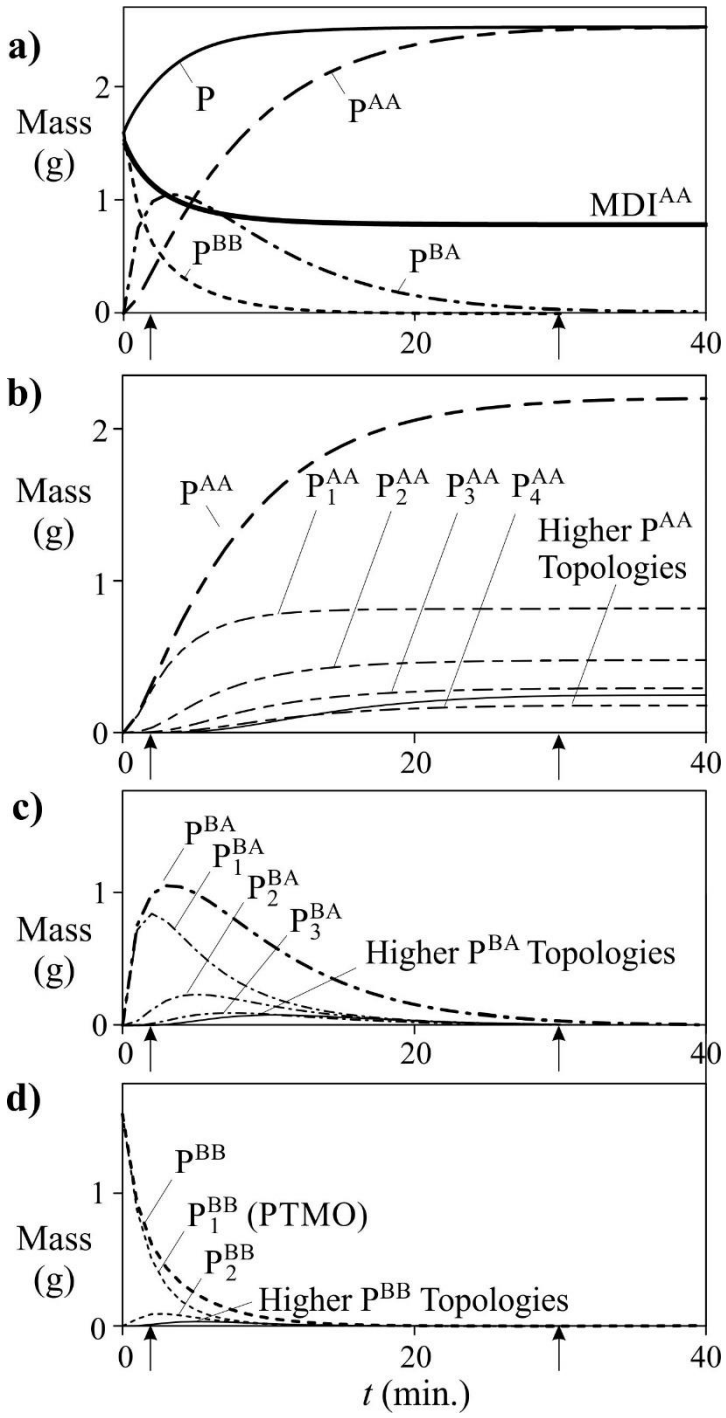

FIGURE 6. Experiment 1: predictions by the double-phases model. Time evolutions of the masses of: a) MDI, total polymer (P), and subsets of polymer species with AA, BA, and BB end groups (P^{AA}, P^{BA}, and P^{BB}); b) P^{AA} and its main contributing topologies; c) P^{BA} and its main topologies; and d) P^{BB} and its main topologies.

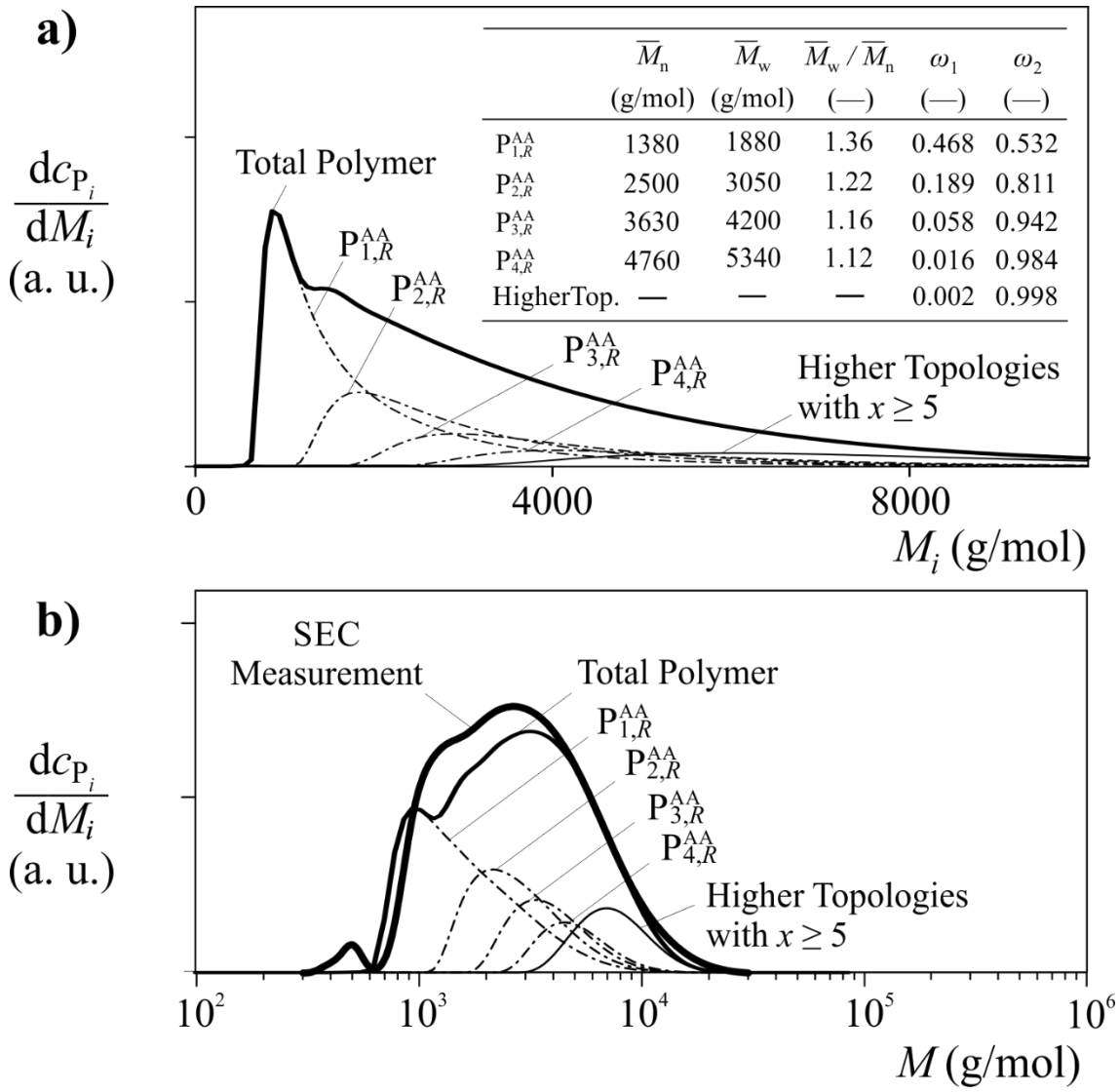

	$\overline{M}_n$ (g/mol)	$\overline{M}_w$ (g/mol)	$\overline{M}_w / \overline{M}_n$ (—)	ω_1 (—)	ω_2 (—)
$P^{AA}_{1,R}$	1380	1880	1.36	0.468	0.532
$P^{AA}_{2,R}$	2500	3050	1.22	0.189	0.811
$P^{AA}_{3,R}$	3630	4200	1.16	0.058	0.942
$P^{AA}_{4,R}$	4760	5340	1.12	0.016	0.984
HigherTop.	—	—	—	0.002	0.998

FIGURE 7. Experiment 1. MMD of the total polymer at t_{end} = 30 min.: measurement and predictions by the double-phases model. Figure 7a show the predicted MMDs (with a linear horizontal axis) of the total polymer and its main topologies. The table presents the average molar masses of the main topologies, with (ω_1, ω_2) representing the weight fractions of the polymer MMD produced in phases 1 and 2, respectively. Figure 7b compares the measured and predicted MMD (with a logarithmic horizontal axis) for the total polymer and main topologies.

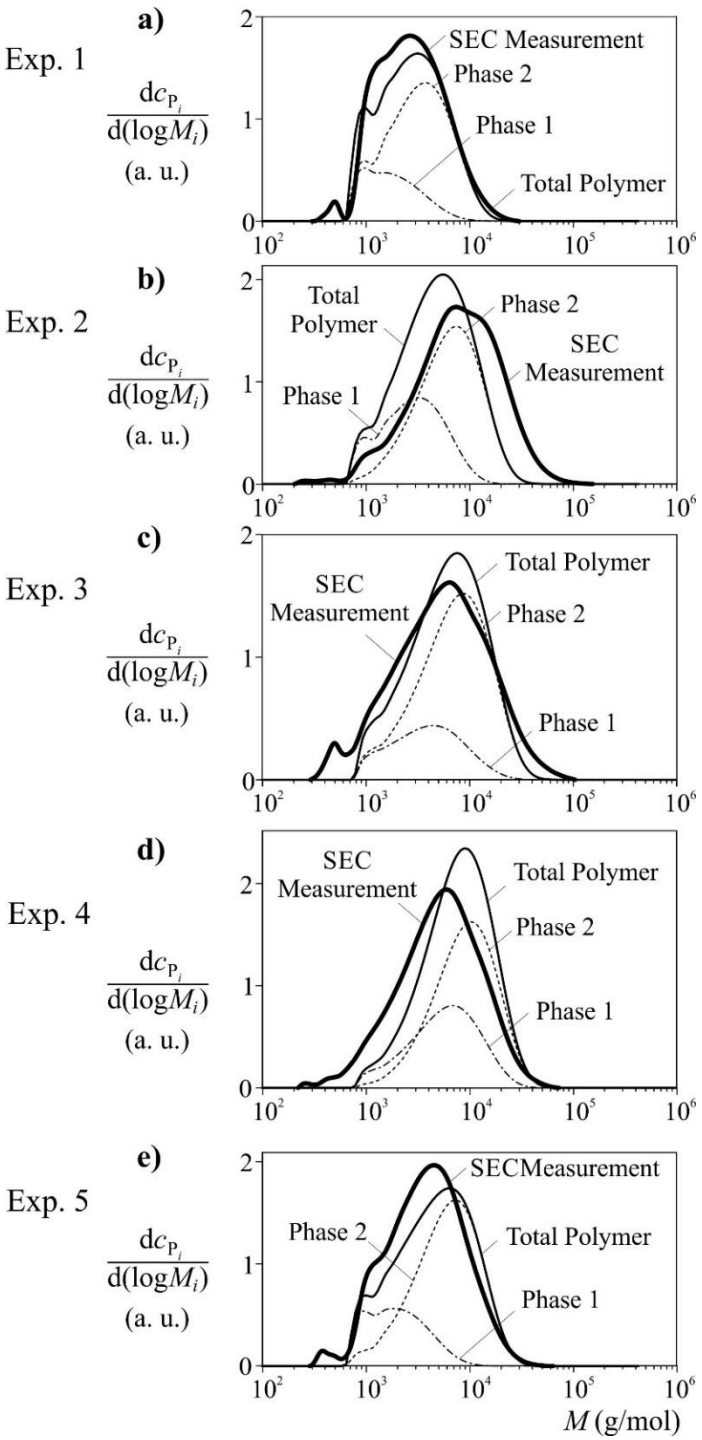

FIGURE 8. Experiments 1-5: final experimental MMDs of the total polymers, and predictions by the double-phases model. The model was adjusted to the measurements of Exp. 1. The total predicted MMDs are composed by a lower MMD produced in phase 1, and a higher MMD produced in phase 2.

Weight MMD of the Final Polymer

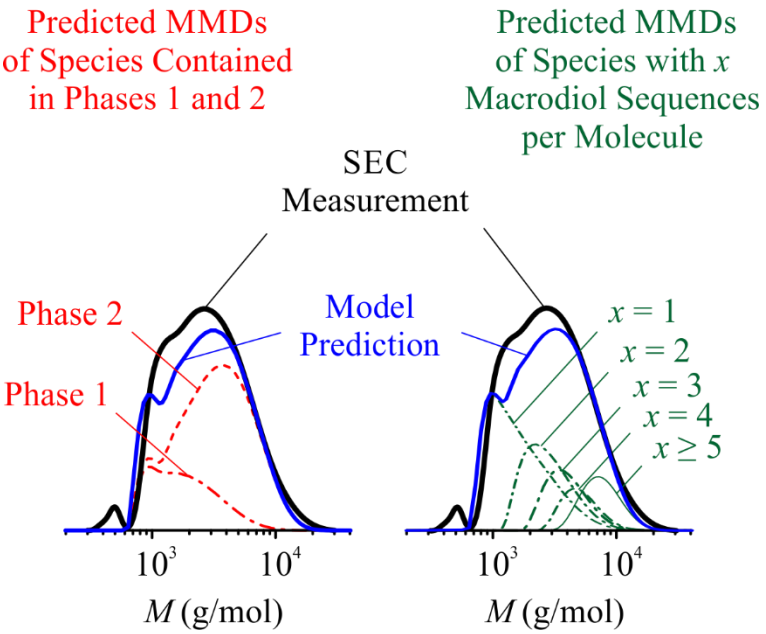

Figure 1

Click here to download Figure Fig1.tif

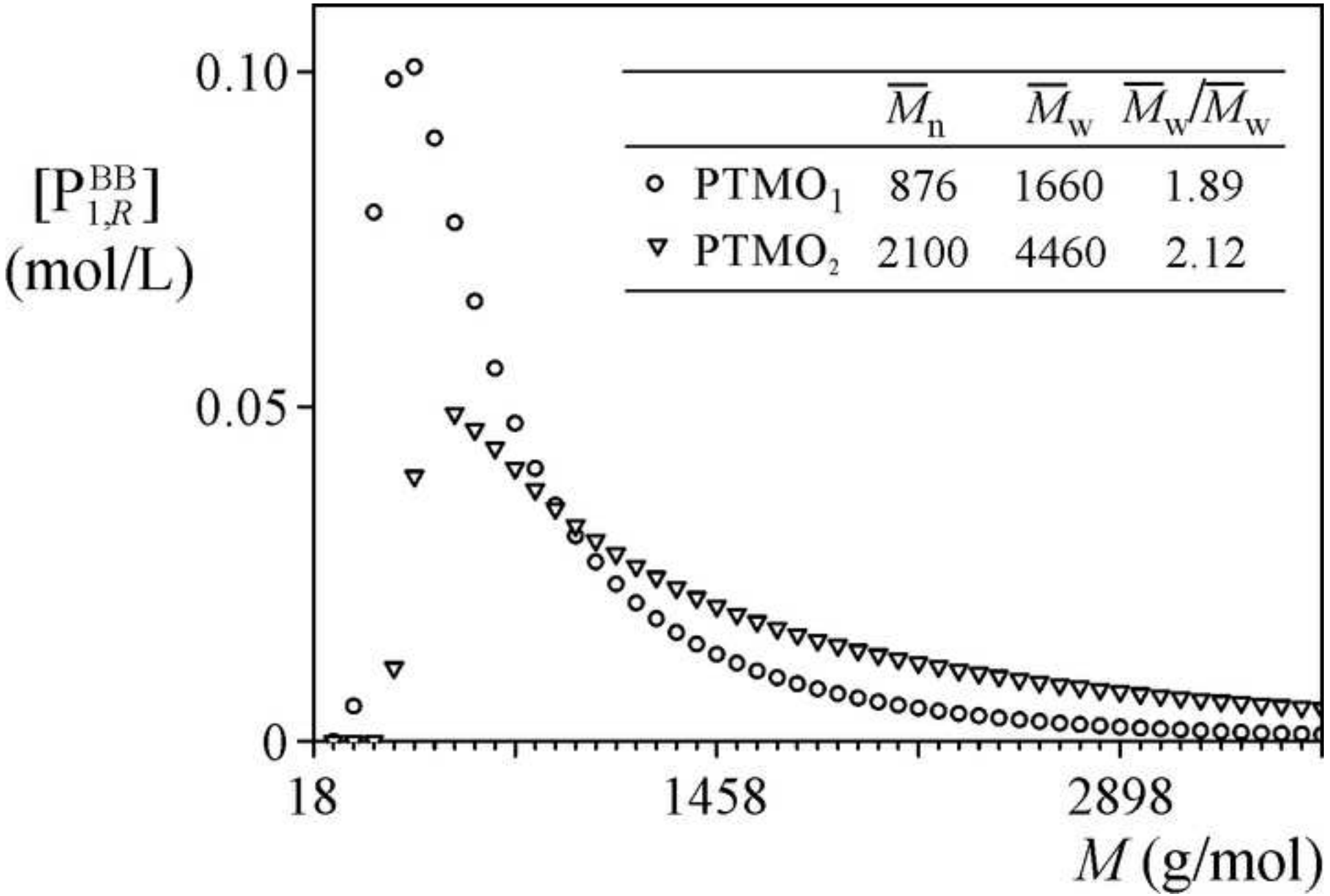

Figure 2

Click here to download Figure Fig2.tif

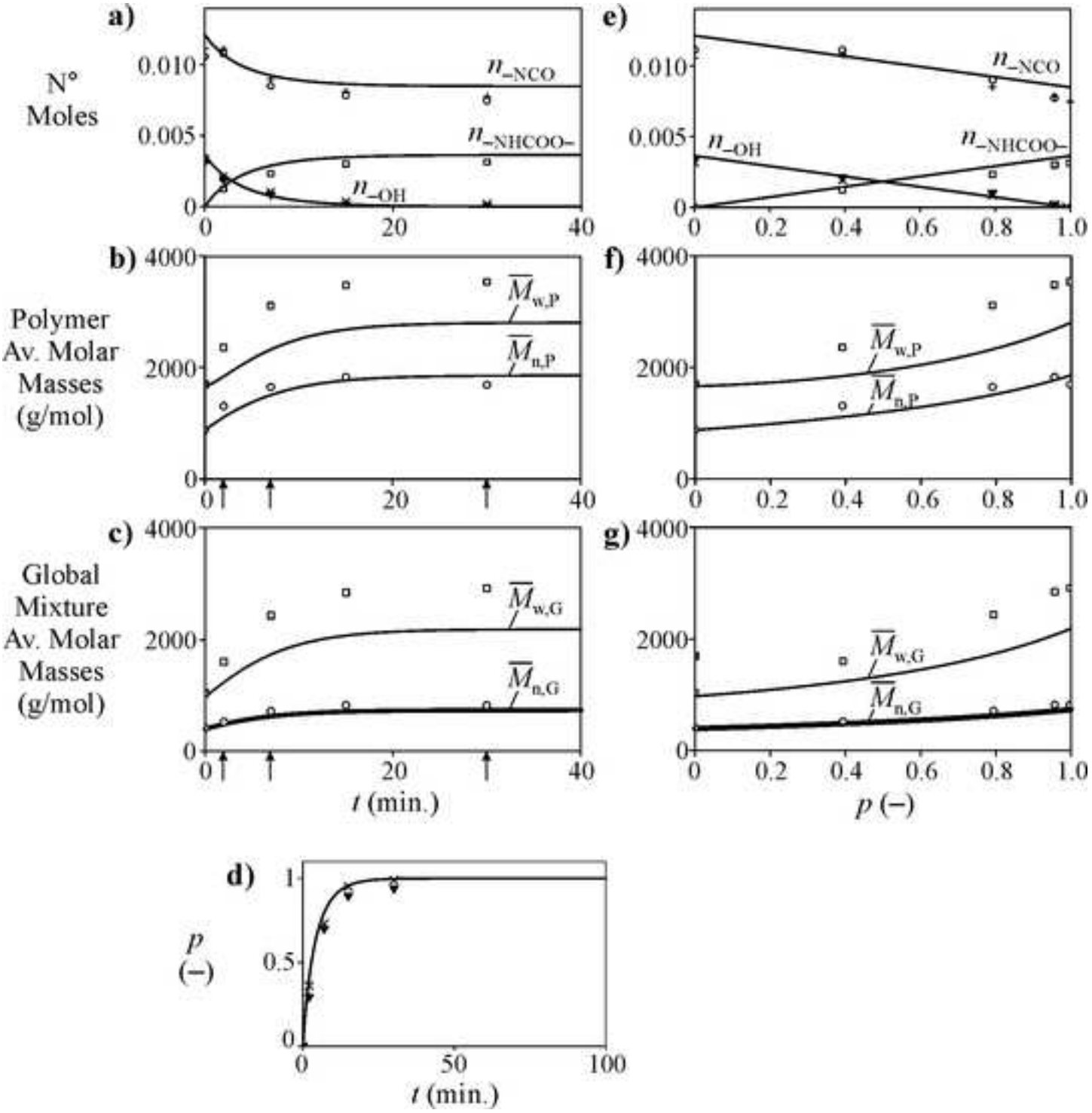

Figure 3

Click here to download Figure Fig3.tif

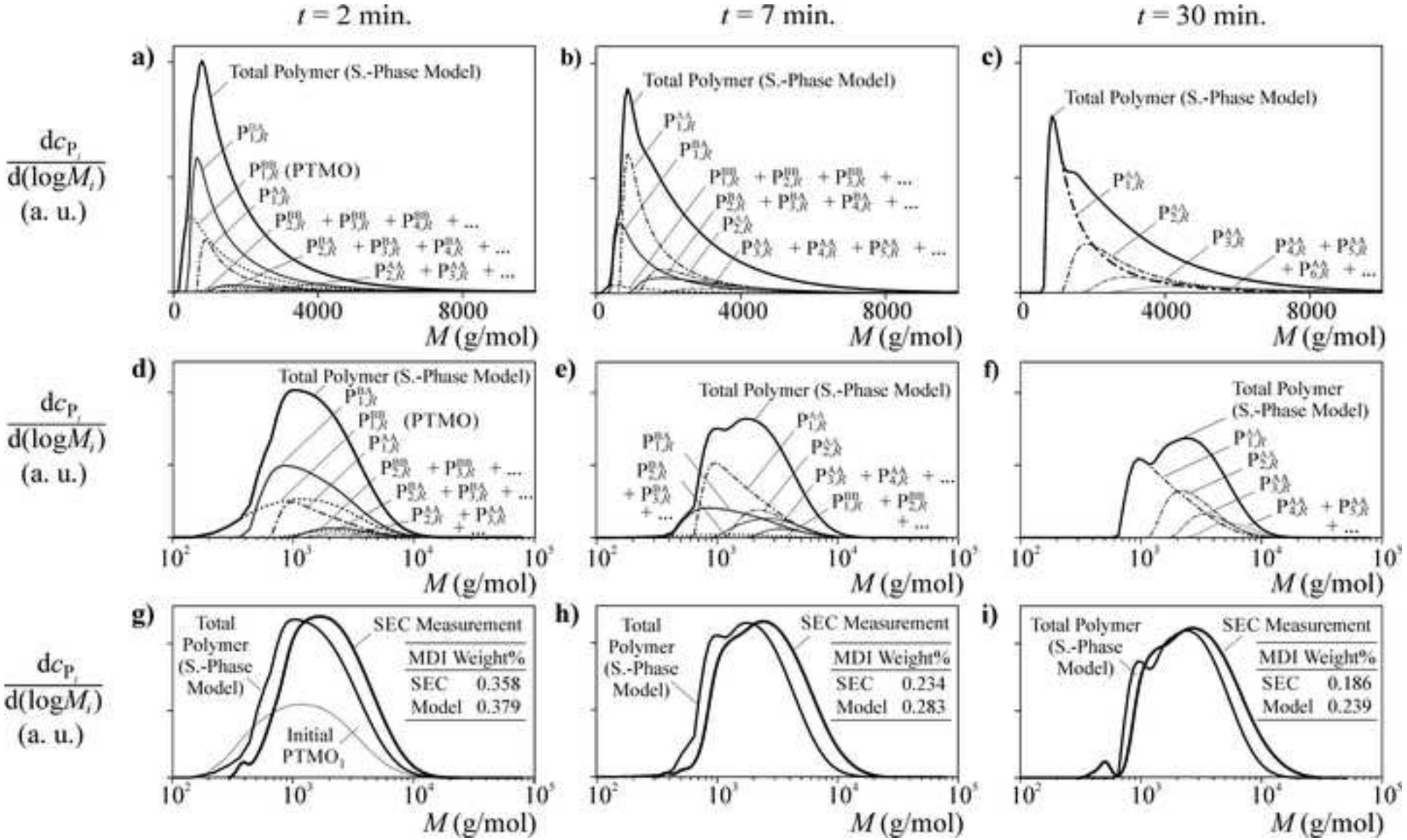

Figure 4

Click here to download Figure Fig4.tif

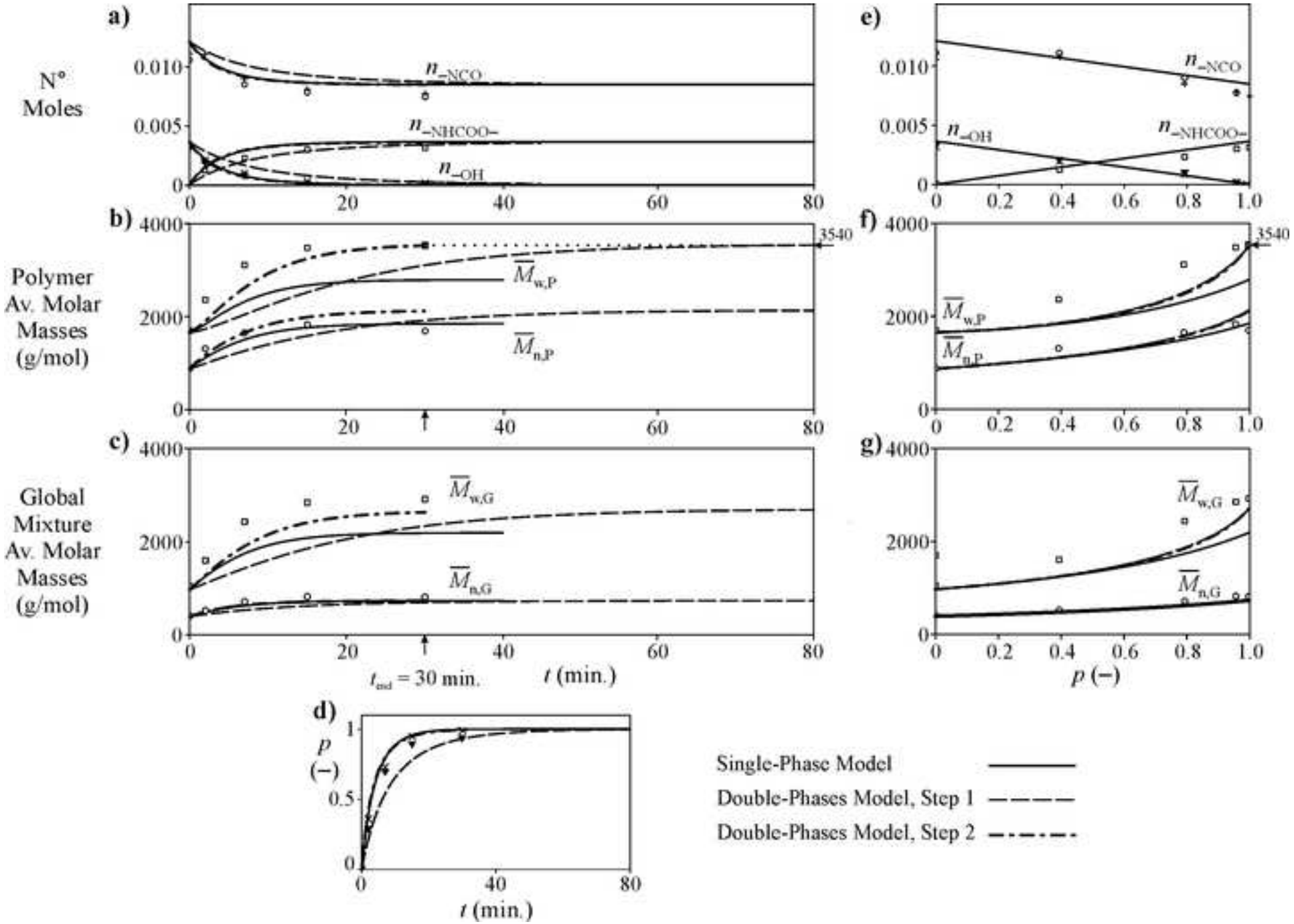

Figure 5

Click here to download Figure Fig5.tif

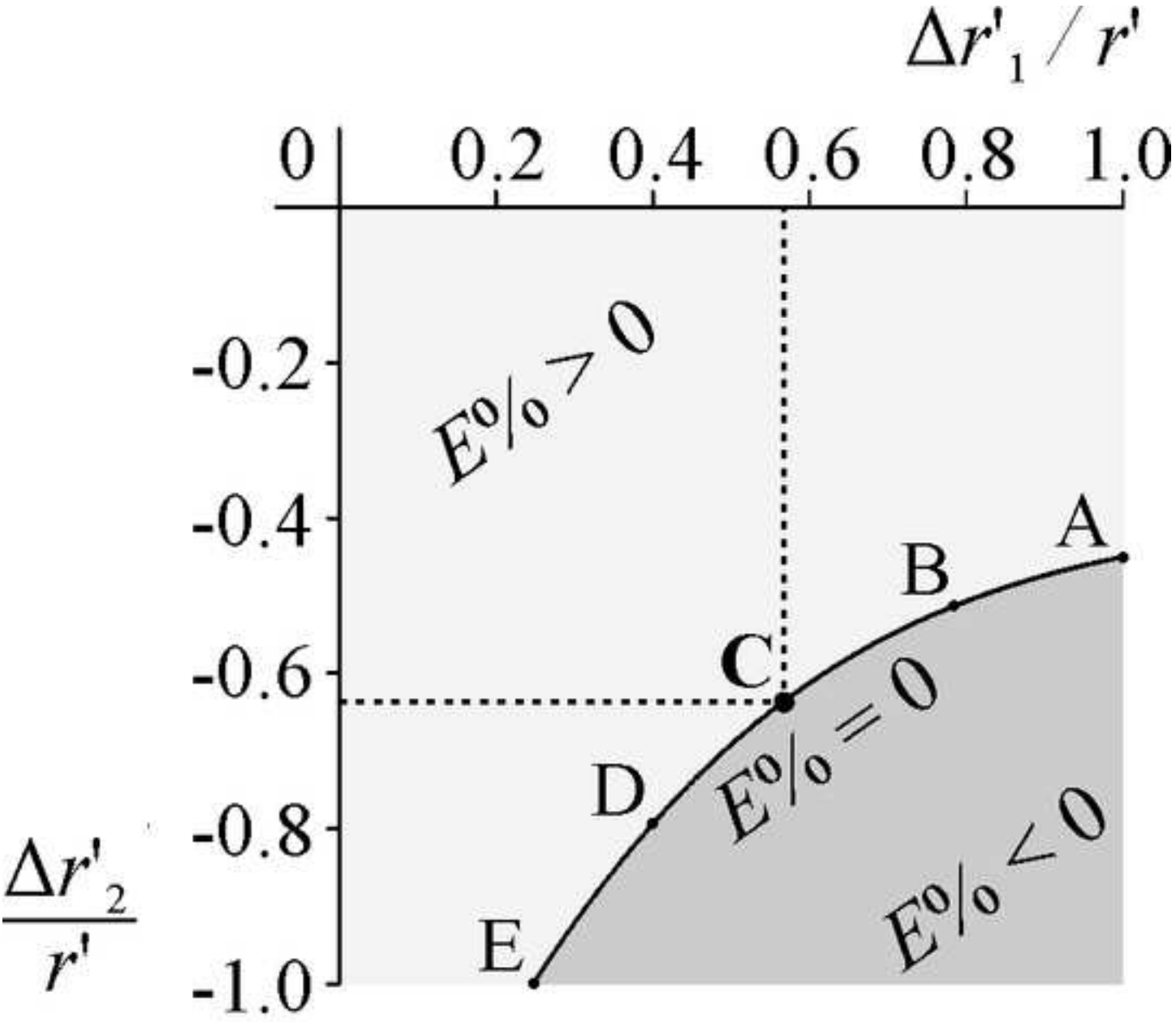

Point	r'_1	r'_2
A	0.000	0.436
B	0.065	0.455
C	**0.130**	**0.494**
D	0.180	0.539
E	0.226	0.600

Figure 6

Click here to download Figure Fig7.tif

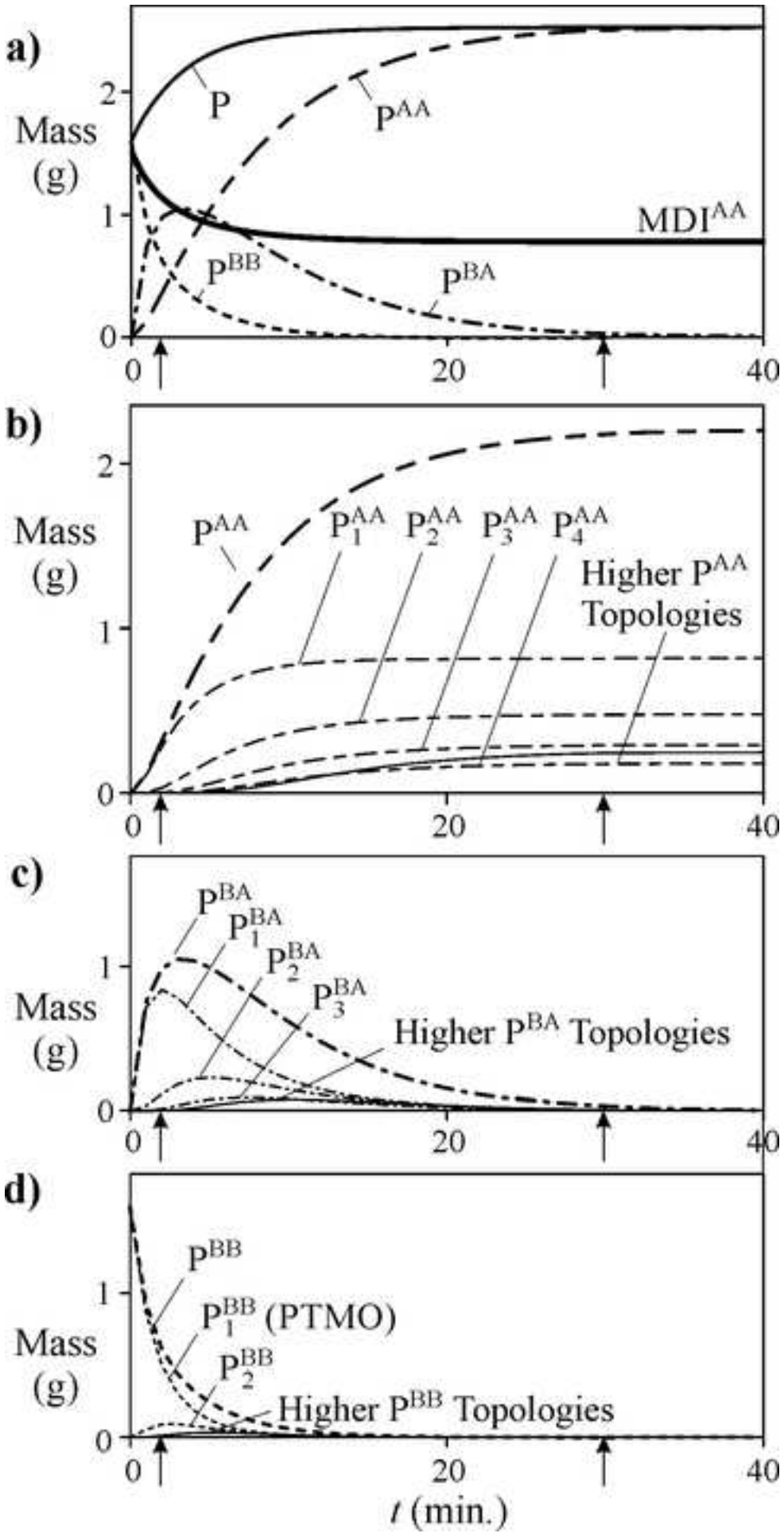

Figure 7

Click here to download Figure Fig8.tif

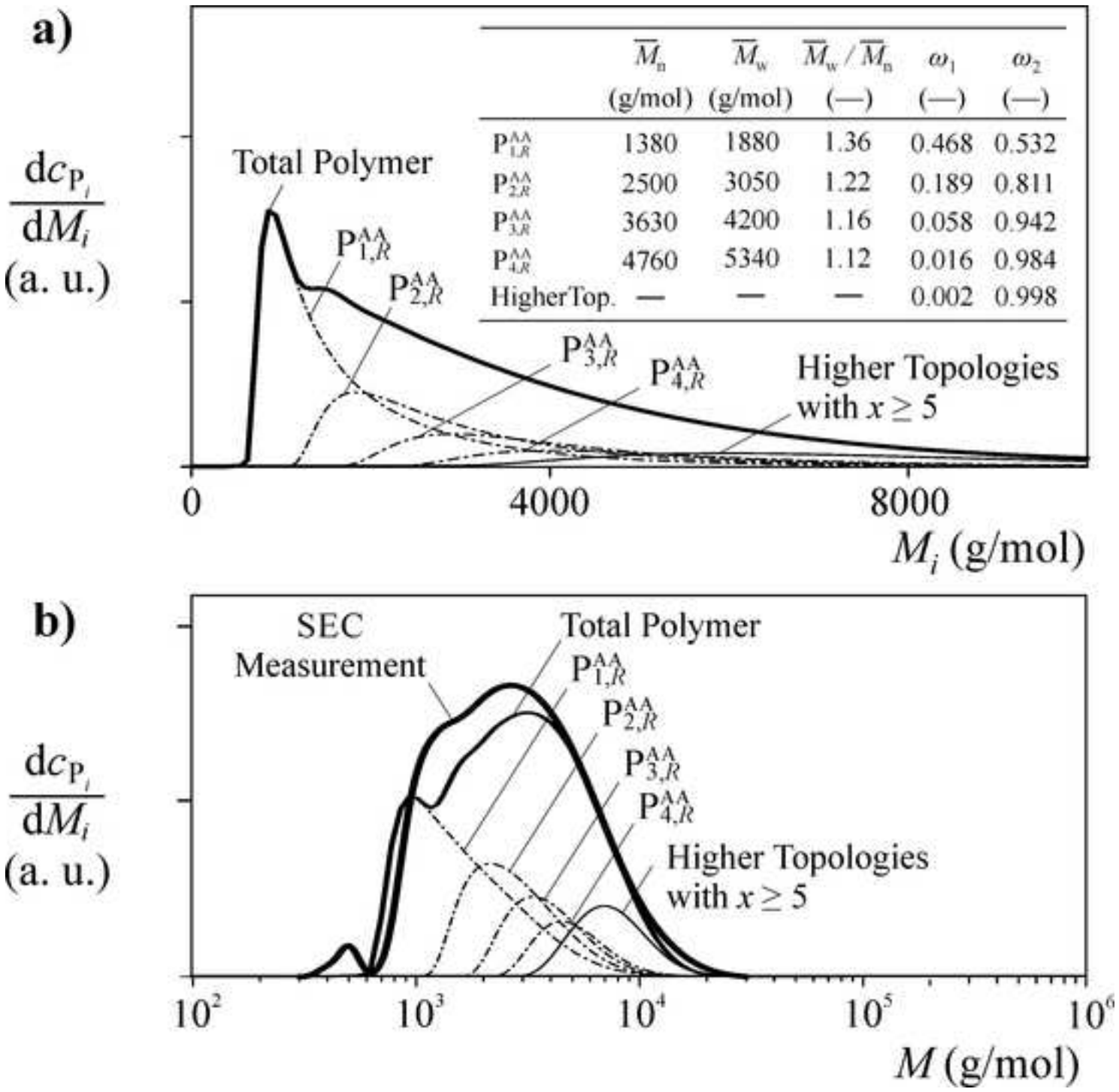

	$\overline{M}_n$ (g/mol)	$\overline{M}_w$ (g/mol)	$\overline{M}_w / \overline{M}_n$ (—)	ω_1 (—)	ω_2 (—)
$P^{AA}_{1,R}$	1380	1880	1.36	0.468	0.532
$P^{AA}_{2,R}$	2500	3050	1.22	0.189	0.811
$P^{AA}_{3,R}$	3630	4200	1.16	0.058	0.942
$P^{AA}_{4,R}$	4760	5340	1.12	0.016	0.984
HigherTop.	—	—	—	0.002	0.998

Figure 8

Click here to download Figure Fig6.tif

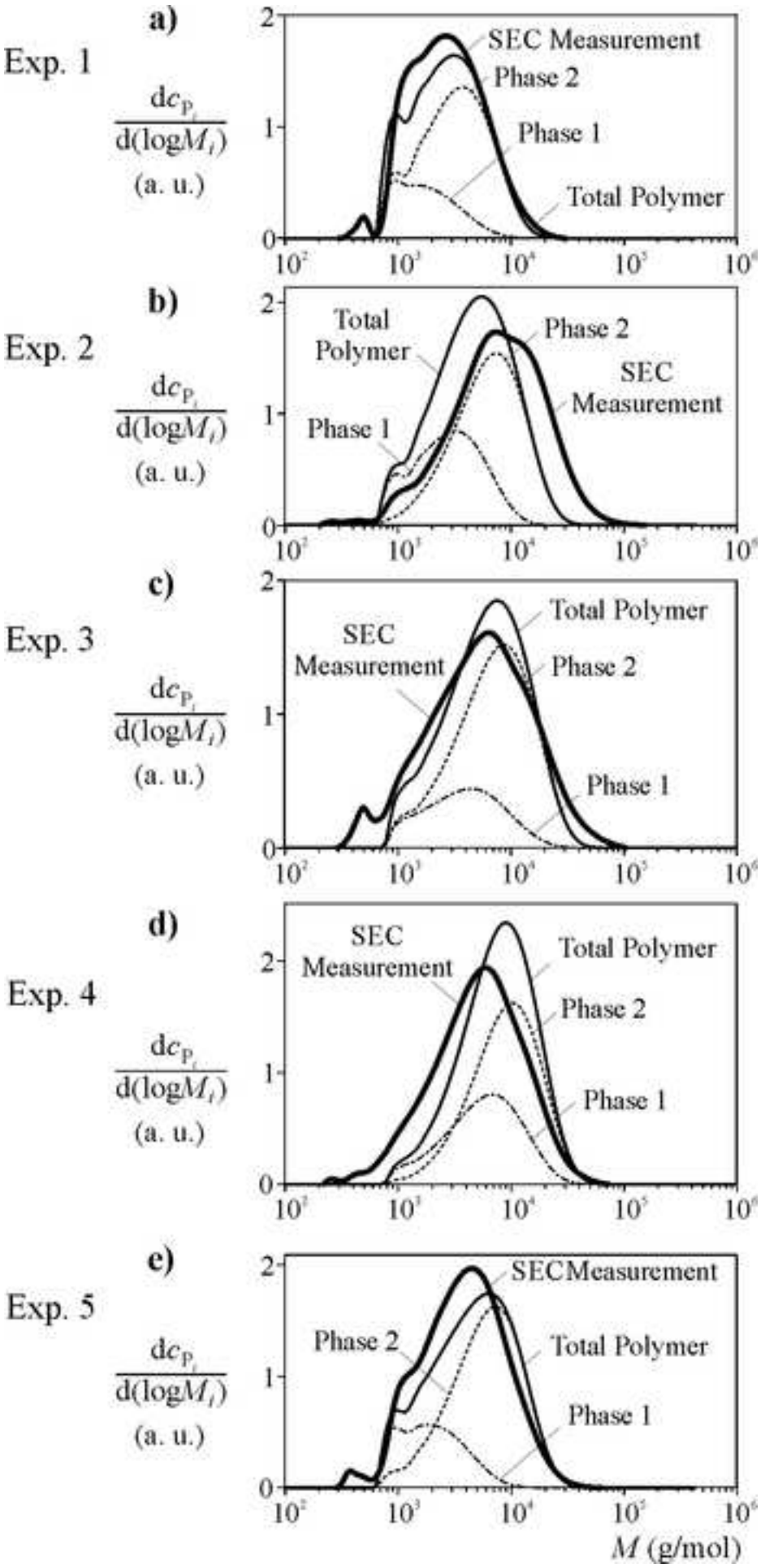

Table 1

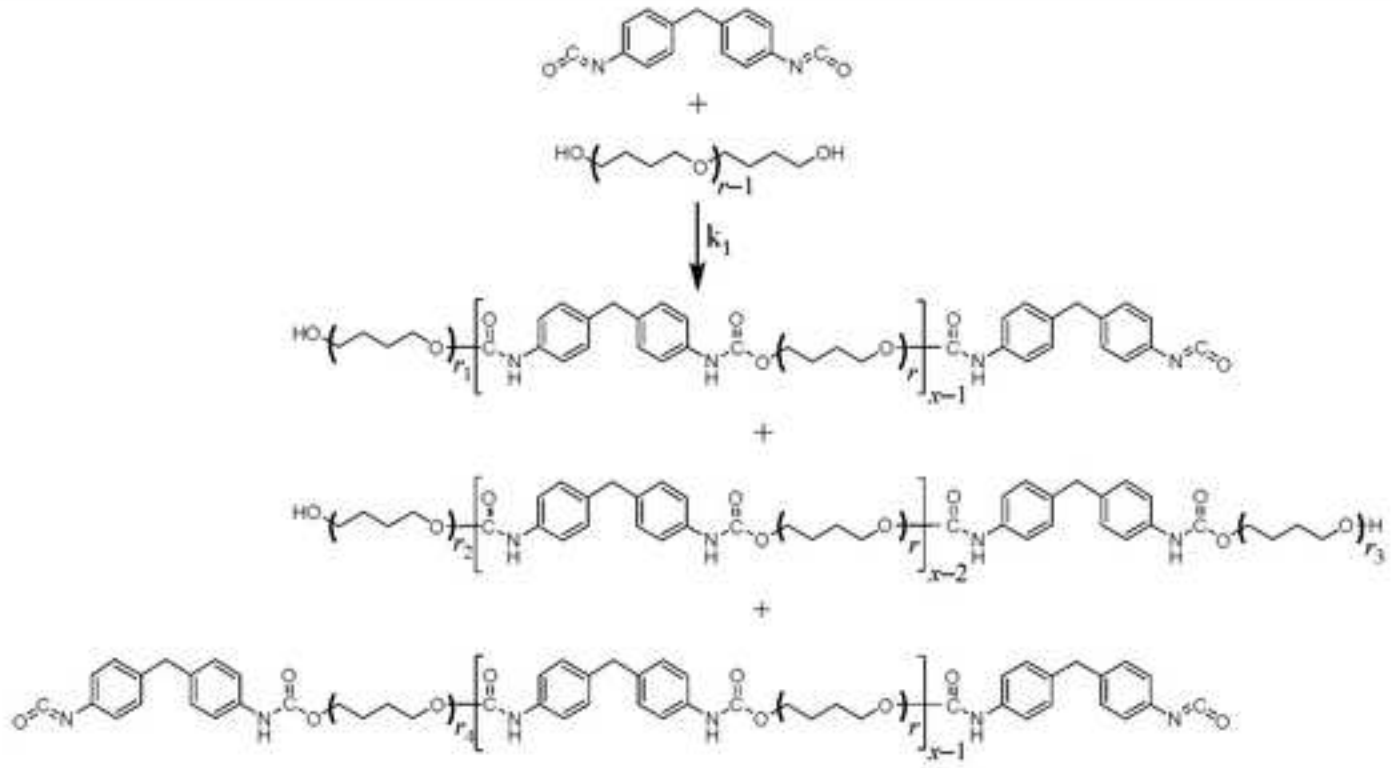

Graphical Abstract Image

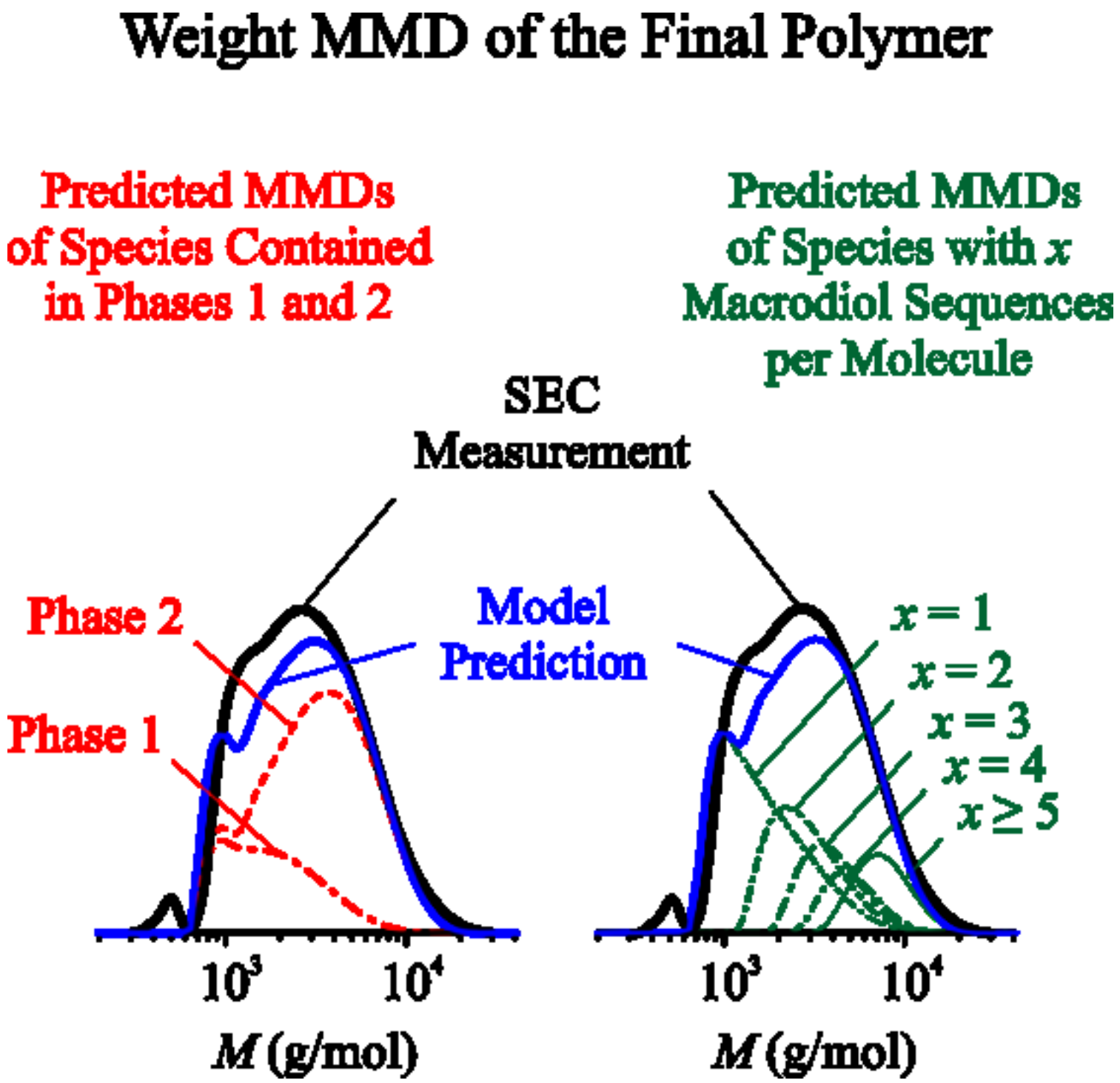

Linear Segmented Polyurethanes. II. A Mathematical Model for the Prepolymerization Stage

Mara L. Polo[1], Juan I. Pesoa[1], Verónica V. Nicolau[2], Marisa E. Spontón[1], Diana A. Estenoz[1], Gregorio R. Meira[1]

[1] INTEC, Universidad Nacional del Litoral and CONICET, (3000) Santa Fe, Argentina.

[2] GPol, Universidad Tecnológica Nacional, Regional San Francisco, (2400) Córdoba, Argentina.

Correspondence to: Gregorio R. Meira (E-mail: *gmeira@santafe-conicet.gov.ar*)

SUPPORTING INFORMATION

TABLE S1. Single-phase model: computational flow-sheet.

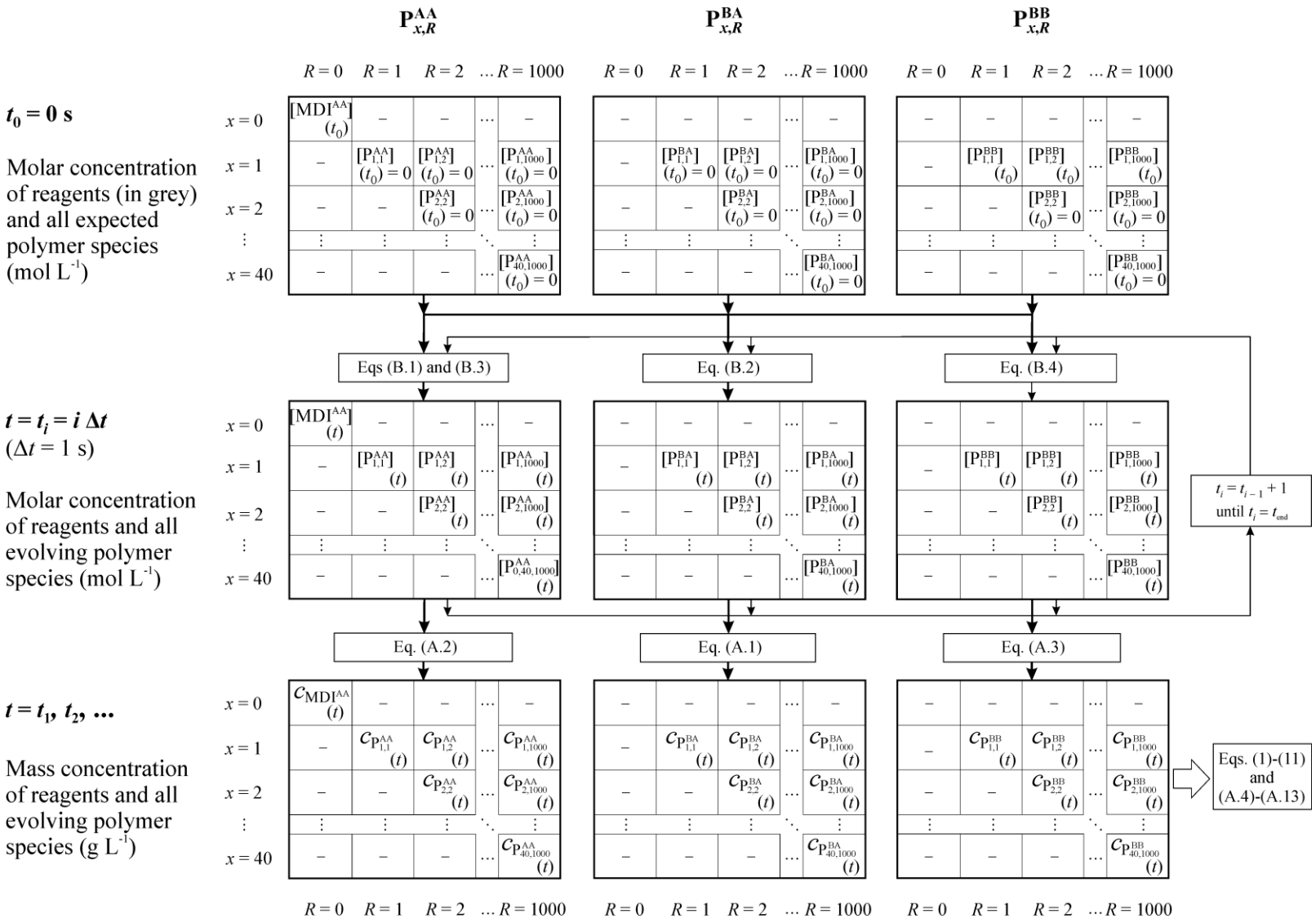

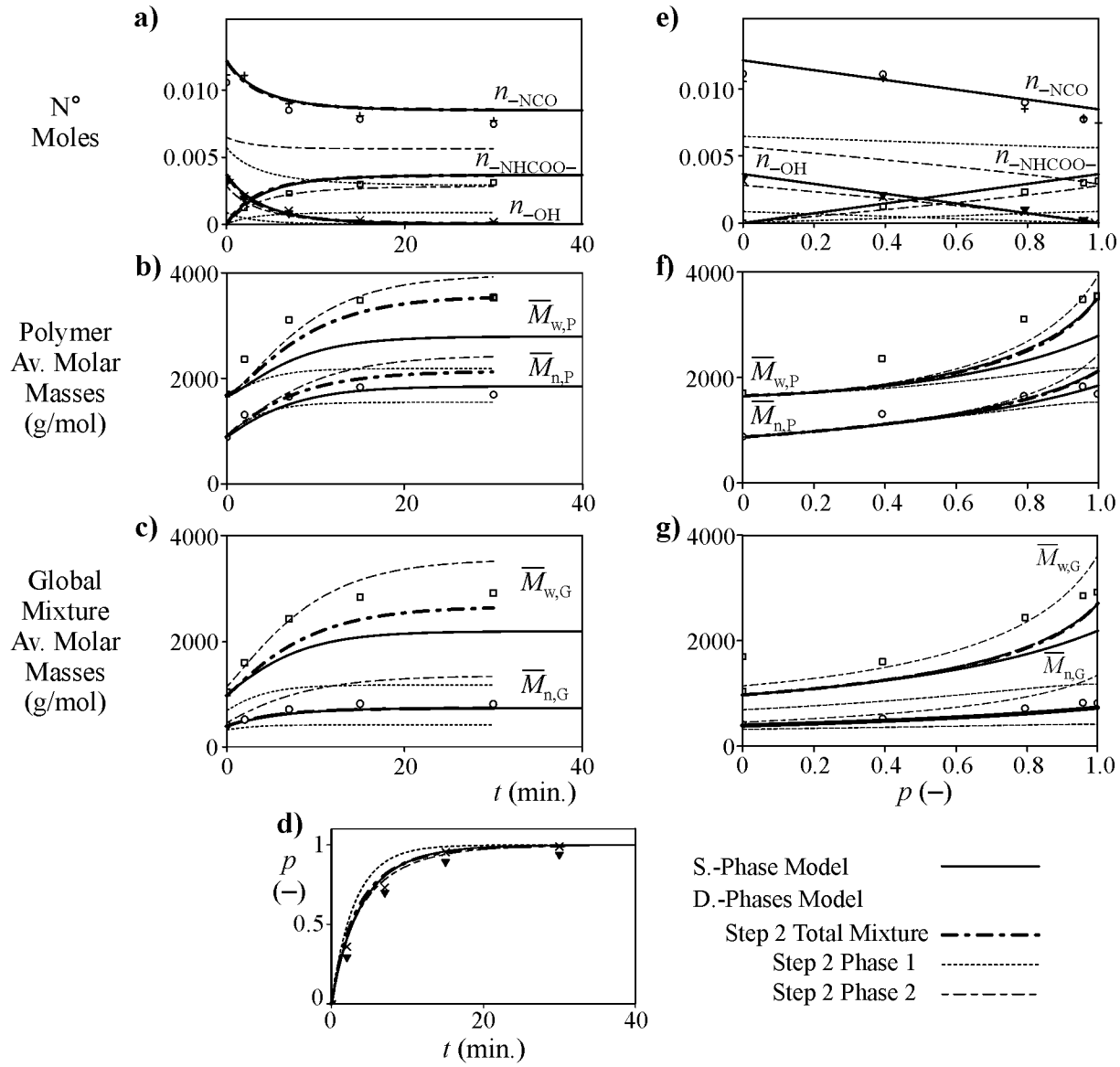

FIGURE S1. Experiment 1: Step 2 of the adjustment procedure of the double-phases model to the measurements of Exp. 1, and comparison with the results of the single-phase model. Compared to Figure 4, this figure also includes the evolution of the predicted variables in phases 1 and 2.